

Emergent Elasticity and Quasiconformal Flow in Active Solids

Nikolas H. Claussen*

Princeton Center for Theoretical Science, Princeton University, Princeton, New Jersey 08542, USA

Fridtjof Brauns†

Max Planck Institute for the Physics of Complex Systems, Nöthnitzer Straße 38, 01187 Dresden, Germany

Max Planck Institute of Molecular Cell Biology and Genetics,

Pfotenhauerstraße 108, 01307 Dresden, Germany and

Center for Systems Biology Dresden, 01307 Dresden, Germany

Boris I. Shraiman‡

Kavli Institute for Theoretical Physics, University of California, Santa Barbara, California 93106, USA

A constitutive relation between stress and strain relative to a reference state is the basic assumption of elasticity theory. However, in living matter, force generation is governed by motor molecule activity, which does not depend on deformation relative to a reference. A different approach is needed to describe how cells sculpt tissues through local active forces. We develop a theory of two-dimensional continuum mechanics where the active stress configuration, rather than a reference shape, is the fundamental input. Motivated by the Active Tension Network model for epithelia, we encode motor-driven forces between cells in a Riemannian *tension metric*. We derive a *stress–metric* relation for the macroscopic stress that results from embedding the tension manifold into physical space (defining cell positions). Despite the absence of constitutive laws, a stress-free reference state and an effective stress-strain relation arise from the tension metric, making the system an effectively elastic *active solid*. Moving from statics to dynamics, our framework describes how an active solid can morph its shape through adiabatic dynamics of active stress. To capture large, plastic deformations through cell rearrangement, we introduce a second metric that geometrizes the cell network topology. Topological rearrangement appears as a continuous reparametrization of the tension manifold. This mathematical framework, based on Riemannian geometry, isothermal coordinates, and quasi-conformal flows, quantitatively predicts how local contractile activity determines large-scale shape and provides a principled continuum description of active plasticity. A companion paper validates the continuum analysis through coarse-graining of discrete cell networks. Our theory identifies a geometric origin of emergent elasticity and plasticity in living matter and, more broadly, in active and granular materials.

INTRODUCTION

During morphogenesis, cells sculpt the physical form of the developing embryo. In contrast to inert materials, living tissues generate forces internally [1, 2]. Key challenges are to characterize the macroscopic mechanical properties (i.e. the “phase of matter”) of developing tissues and to understand the control of tissue shape (morphogenesis) by the cell-generated forces.

Conventional elasticity, based on a reference shape and a constitutive law relating stress and strain (rate) [3], has served as the starting point for much work on tissue mechanics [4–6]. For instance, epithelial cells are often described as having a target area and perimeter [7] with deformation from a target shape defining the stress. However, biological observations challenge this paradigm. First, the turnover of the force-bearing molecules in cells, rapid compared to morphogenetic timescales, allows the “rest length” of a cell to change [8], ruling out a fixed

reference state. Since stress needs to be actively maintained against relaxation due to turnover, one expects active stresses to dominate on long timescales. Active stress, however, is not controlled by strain but by the activity of molecular motors, such as myosin. Nevertheless, tissues can maintain a macroscopic shape against external shear forces, and, more remarkably, change shape by internally controlled cell rearrangement during morphogenesis. We refer to such a system, which has neither a reference state nor a constitutive law, as an *active solid*.

We therefore seek to understand tissue mechanics by starting from the specification of cell-associated active stress instead of a reference shape. The timescale of mechanical equilibration (seconds [9]) is well separated from that of morphogenetic remodeling (hours). One thus expects cells to adjust their shapes and positions to achieve force balance by rearranging local sources of active stress. Morphogenesis takes the form of an adiabatic transformation between force-balanced states, controlled by changes in the local mechanical activity.

More precisely, we are motivated by the study of confluent, two-dimensional epithelia. Here, the dominant, tensile forces are generated along apical adherens junctions (cell-cell interfaces), which act as microscopic muscles [10, 11]. This picture is made precise by the active

* nc1333@princeton.edu

† fbrauns@pks.mpg.de

‡ shraiman@ucsb.edu

tension network (ATN) model [10], a minimal model for epithelial mechanics. Within this framework, we can ask how cells control tissue shape through local active tensions.

To build intuition, consider a conventional fluid foam. Here, a “cell” (foam bubble) interface has no rest length since its tension is independent of its length, set instead by the fluid’s surface tension. These surface tensions are balanced against internal pressure in the foam bubbles. Remarkably, even though microscopically fluid, the foam macroscopically behaves like an elastic solid – it can maintain its shape against gravity [12]. In a foam, interfacial tensions are fixed material parameters. In a tissue, they are promoted to active, dynamical variables (under local cellular control), enabling richer behavior.

We will represent the configuration of tensions by a Riemannian metric \mathbf{g} , a continuum version of Maxwell–Cremona force tessellations [13, 14]. The cell tiling defines an embedding of the tension metric into physical space. We show that the central elements of elasticity theory, a stress-free reference state and a stress-strain relationship, emerge from this embedding. Additionally, we will demonstrate that cell-scale topological rearrangements that enable large deformations can be captured in the continuum theory via a suitable reparametrization of the tension metric. Taken together, these ideas enable a continuum description of adiabatic tissue flow driven by active stress dynamics. The resulting theory is distinct from existing, active fluid models for morphogenesis [15–17], and makes differing, experimentally verifiable predictions for mechanical stress and the effect of motor molecule activity. In a companion paper [18], we show that the continuum-based, “top-down” approach presented here precisely matches a “bottom-up” coarse-graining analysis of the ATN model.

The remainder of this paper is structured as follows. We begin by briefly reviewing the cell-level ATN model. In Section A, we explain how we describe cell tiling and tension configuration in the continuum limit. Section B studies the static problem, and Section C turns to the adiabatic dynamics of active stress. Finally, Sect. D considers topological cell rearrangement.

Discrete theory: 2d tension networks

The microscopic ATN model [10] describes a 2d tiling of cells i, j, \dots whose mechanics is dominated by tensions τ_{ij} along cell-cell interfaces and intracellular pressure p_i (Fig 1, bottom). Accordingly, the differential of elastic energy is given by $dE = -\sum_{ij} \tau_{ij} dl_{ij} + \sum_i p_i dA_i$, where l_{ij}, A_i are interface lengths and cell areas. In mechanical balance, $dE = 0$. We assume that the cells’ positions \mathbf{r}_i are constrained to a fixed two-dimensional surface, and that the cells do not exert traction forces on a substrate (therefore, the tissue-internal forces balance among themselves). This picture applies, for example, to the early *Drosophila* and chicken embryonic epithelia,

which sit atop a liquid yolk and are constrained in the third dimension by the egg shell [1]. The pressures p_i are determined by a local equation of state $p_i = P(A_i)$. (The original ATN model [10] assumed uniform p_i). By contrast, the tensions τ_{ij} are dynamical variables determined by intrinsic motor molecule activity. This is the key premise of the ATN model [10, 19].

Tissue dynamics unfolds on three distinct time scales. The speed of relaxation to mechanical equilibrium is the most rapid, on the order of seconds [9]. Turnover of force-bearing proteins within a few minutes sets the speed of relaxation of passive elastic stress in the cytoskeleton [20]. Finally, morphogenetic remodeling and regulation of contractile activity take place over tens of minutes to hours. Here, we exploit this hierarchy and consider only the dynamics at the slowest, morphogenetic timescale. We therefore assume that the ATN model is in instantaneous mechanical equilibrium and that transient passive stresses relax rapidly. In this limit, the interfacial tensions τ_{ij} are purely determined by local motor activity and *independent* of interface lengths l_{ij} – there are no reference lengths and no constitutive laws for tensions.

In this stress-first setting, we aim to understand how active tensions determine the physical configuration of the cell tiling in force balance, and how this configuration evolves when tensions change adiabatically. To this end, it will be useful to think of the tension configuration as a network dual to the cell tiling. Since the cells generically meet at 3-fold vertices, the tensions form an intrinsically defined triangulation with one node per cell i and a length τ_{ij} edge between neighbors i and j ; Fig. 1. Each tricellular vertex ijk corresponds to one “tension triangle”, the shape of which encodes the local tension configuration (for example, tension anisotropy). This Maxwell–Cremona-like “tension triangulation” serves as a point of departure for our analysis.

RESULTS

A. Continuum description of ATNs by Riemannian geometry

1. Tension metric and macroscopic stress tensor

A triangulation, intrinsically specified by its adjacency graph and edge lengths, defines a (piecewise-linear) metric surface (see Fig. 1, top). We can therefore coarse-grain the tension triangulation to a continuous tension manifold with *tension metric* $g_{\alpha\beta}(\boldsymbol{\xi})$ as a function of Lagrangian coordinates $\boldsymbol{\xi}$, which play the role of the cell labels i, j . This continuum limit is well-defined as long as the microscopic tensions form non-degenerate triangles [21]. For an infinitesimal line element $d\boldsymbol{\xi}$, the tension metric yields the tension $d\tau$ on cell interfaces oriented *transverse* to it as $d\tau^2 = g_{\alpha\beta}(\boldsymbol{\xi}) d\xi_\alpha d\xi_\beta$. In the “microscopic limit” where $d\boldsymbol{\xi}$ connects two adjacent triangulation nodes, $d\tau$ is the tension along the interface

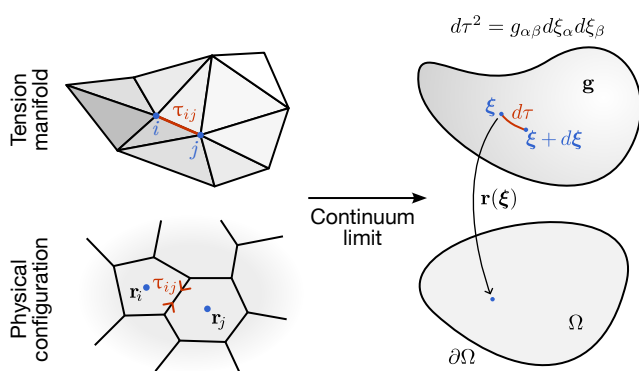


FIG. 1. A triangulation (left) is a discrete Riemannian surface. The tension metric defines junctional tensions. An embedding of the metric into physical space is the continuum equivalent of the centroids in the cell tessellation.

between the corresponding cells.

A set of physical cell positions $\mathbf{r}(\boldsymbol{\xi})$ now defines a map from the tension manifold into two-dimensional physical space, to which we refer as the “embedding” (Fig. 1, bottom). For simplicity, we assume that physical space is the plane, but our theory readily generalises to tissues on arbitrary curved surfaces. Under the map $\mathbf{r}(\boldsymbol{\xi})$, the tension metric \mathbf{g} transforms as

$$g_{\alpha\beta}(\mathbf{r}) = \frac{\partial \xi_\gamma}{\partial r_\alpha} g_{\gamma\delta}(\boldsymbol{\xi}) \frac{\partial \xi_\delta}{\partial r_\beta} \quad (1)$$

In the following, we non-dimensionalize $\mathbf{g} \mapsto p_0^2 \mathbf{g}$ so the metric has units of $[\text{length}]^{-2}$. The dimensional factor p_0 converts units of line tension to units of length, and will be identified as the reference pressure below.

Note that different triangulations (i.e., local tension configurations) can realize the same tension manifold. For instance, all triangulations of the plane realize the Euclidean metric. The tension triangulation thus encodes “microscopic” information in addition to the tension metric \mathbf{g} ; we return to this point systematically in Sect. D. One important additional degree of freedom is the local cell density $n(\boldsymbol{\xi}) d^2 \xi$, the number of cells (triangulation nodes) per unit area. The cell density determines the continuum pressure field p (the equivalent of the intracellular pressures p_i) via an equation of state $p = P(n)$. In contrast to the active tensions, we hence treat pressure as a *passive* field. We define a reference cell density n_0 by $P(n_0) = p_0$. Under $\mathbf{r}(\boldsymbol{\xi})$, the density transforms as $n(\mathbf{r}) = n(\boldsymbol{\xi}) \det[\partial \boldsymbol{\xi} \mathbf{r}]$, and therefore:

$$p(\mathbf{r}) = P(n(\boldsymbol{\xi}) \det[\partial \boldsymbol{\xi} \mathbf{r}]) \quad (2)$$

We now link the geometry of the tension metric and the embedding to mechanics. The macroscopic Cauchy stress tensor of an active solid is the sum of two contributions

$$\sigma_{\alpha\beta}^{\text{tot}} = \sigma_{\alpha\beta} - p \delta_{\alpha\beta} \quad (3)$$

where $p \delta_{\alpha\beta}$ is the isotropic pressure, and $\sigma_{\alpha\beta}$ is the tensile stress due to the τ_{ij} .

The Cauchy stress tensor relates the infinitesimal force $d\mathbf{f} = \boldsymbol{\sigma} \cdot \mathbf{n} dr$ acting on a virtual cut with the cut’s unit normal \mathbf{n} and length dr in the physical configuration. To see how the tension metric determines $\boldsymbol{\sigma}$, consider two adjacent cells at \mathbf{r} and $\mathbf{r} + d\mathbf{r}$ (we implicitly set dr to be of the scale of a single cell, infinitesimal in the continuum limit). The magnitude of the force $d\mathbf{f}$ acting through the virtual cut $d\mathbf{r}$ (Fig. 2) equals the tension $|d\mathbf{f}| = d\tau$ along the interface between the two cells. It is determined by the tension metric, $d\tau^2 = p_0^2 g_{\alpha\beta}(\mathbf{r}) dr_\alpha dr_\beta$. On the other hand, the stress tensor applied to the cut normal yields $d\mathbf{f} = \boldsymbol{\sigma} \cdot \mathbf{n} dr = \boldsymbol{\sigma} \cdot \boldsymbol{\epsilon} \cdot d\mathbf{r}$, where $\boldsymbol{\epsilon}$ is the antisymmetric tensor and \cdot is the standard Euclidean dot product. Equating tension- and cell-space expressions:

$$\begin{aligned} p_0^2 d\mathbf{r}^T \cdot \mathbf{g}(\mathbf{r}) \cdot d\mathbf{r} &= d\tau^2 = d\mathbf{r}^T \cdot (\boldsymbol{\epsilon}^T \cdot \boldsymbol{\sigma}^2(\mathbf{r}) \cdot \boldsymbol{\epsilon}) \cdot d\mathbf{r} \\ \Rightarrow \boldsymbol{\sigma}^2(\mathbf{r}) &= p_0^2 \boldsymbol{\epsilon}^T \cdot \mathbf{g}(\mathbf{r}) \cdot \boldsymbol{\epsilon} \end{aligned} \quad (4)$$

Since equality holds for arbitrary $d\mathbf{r}$, the stress tensor must be the matrix square root of the metric, rotated by $\pi/2$, and scaled by p_0 . We refer to Eq. (4) as the *stress-metric relation*. It links the microscopic stress, encoded in the tension metric, to the macroscopic stress tensor, defined in physical space. Thus, it replaces the stress-strain relation of a conventional elastic solid.

Eq. (4) depends on the cell embeddings $\mathbf{r}(\boldsymbol{\xi})$, which are physical observables, not mere coordinates [22]. Of particular interest are mechanically equilibrated embeddings, which must fulfill force balance:

$$\partial_\alpha \sigma_{\alpha\beta}^{\text{tot}} = \partial_\alpha \sigma_{\alpha\beta} - \partial_\beta p = 0 \quad (5)$$

Physically, tensile forces $\partial_\alpha \sigma_{\alpha\beta}$ must balance against pressure gradients $\partial_\beta p$. From Eqs. (4) and 5 we can already anticipate a special role for a configuration $\mathbf{r}(\boldsymbol{\xi})$ where the tension metric is isotropic. In such an *isothermal configuration*, $\boldsymbol{\sigma}$ is isotropic and trivially balanced by pressure, defining an emergent stress-free reference configuration. Appendix A illustrates the link between the cell-level and the above continuum formulation for the toy problem of a uniform “rectangular foam.”

Equations (4) and (5), supplemented with mechanical boundary conditions (BCs), set the physical configuration (cell positions) $\mathbf{r}(\boldsymbol{\xi})$ for a given tension metric $\mathbf{g}(\boldsymbol{\xi})$ and cell density $n(\boldsymbol{\xi})$. In the following, we introduce a mathematical framework to solve Eqs. (4)–(5) and determine when (stable) force-balanced states exist. We first study the statics problem to see how tissue shape and response to external forces emerge from fixed $\mathbf{g}(\boldsymbol{\xi})$. Then, we turn to quasi-static shape dynamics due to changes of $\mathbf{g}(\boldsymbol{\xi})$, and finally generalize our framework to describe plastic flow (cell rearrangement).

2. Complex coordinates and (quasi)conformal maps

To solve Eq. (5), we use complex coordinates $z = z_1 + iz_2$. Complex notation converts matrix to scalar algebra

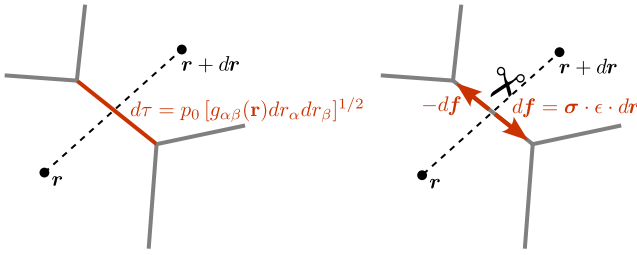


FIG. 2. Left: In the continuum limit, the displacement vector between two cell centroids becomes a differential dr . The tension metric determines the tension $d\tau$ on the interface between these cells. In isothermal coordinates, $dr = p_0^{-1} d\tau$. Right: The stress tensor σ is defined by the traction forces that act through infinitesimal virtual cuts. A cut along dr must yield the interfacial tension, relating tension metric and stress tensor in Eq. (4).

and greatly simplifies the description of conformal maps, which will play an important role. A symmetric matrix \mathbf{q} (e.g. the metric \mathbf{g}) defines a quadratic form $\mathbf{v} \mapsto q_{\alpha\beta} v^\alpha v^\beta$ which becomes

$$4q_{\alpha\beta} v^\alpha v^\beta = (q_{z\bar{z}} + q_{\bar{z}z})v\bar{v} + q_{zz}\bar{v}\bar{v} + q_{\bar{z}\bar{z}}v v, \quad (6a)$$

$$\text{where } q_{z\bar{z}} = q_{\bar{z}z} = q_{11} + q_{22} = \text{Tr } \mathbf{q},$$

$$q_{zz} = q_{\bar{z}\bar{z}} = q_{11} - q_{22} + 2iq_{12} \quad (6b)$$

The *Beltrami coefficient* μ_q is defined by:

$$\mu_q = \frac{q_{zz}}{q_{z\bar{z}} + \sqrt{q_{z\bar{z}}^2 - |q_{zz}|^2}} = \frac{q_{zz}}{\text{Tr } \mathbf{q} + 2\sqrt{\det \mathbf{q}}} \quad (7)$$

Since q_{zz} is the deviatoric component of \mathbf{q} , it measures the relative anisotropy.

Note that as a *coordinate*, the complex number $z = z_1 + iz_2$ contains the same information as the Cartesian vector $(z_\alpha) = \mathbf{z} = (z_1, z_2)$. We use the two interchangeably. However, it is convenient to write *functions* f as $f(z, \bar{z})$ with formally independent variables z, \bar{z} . With this convention, vector calculus can be expressed in terms of the Wirtinger derivatives $\partial_z = (\partial_1 - i\partial_2)/2$, $\bar{\partial}_z = (\partial_1 + i\partial_2)/2$. For example, for real-valued potentials θ, ψ , $2\bar{\partial}_z \theta$ is the gradient, while $2i\bar{\partial}_z \psi$ is a solenoidal vector field. The Euclidean Laplace operator is $4\partial_z \bar{\partial}_z = \partial_1^2 + \partial_2^2 =: \Delta$. The Jacobian matrix $\mathbf{D}f$ of a map $f(z, \bar{z})$ reads

$$\mathbf{D}f = \begin{bmatrix} \partial_z f & \bar{\partial}_z f \\ \partial_z \bar{f} & \bar{\partial}_z \bar{f} \end{bmatrix} \quad (8)$$

Note that the matrix entries in Eq. (8) are not in Cartesian z_1, z_2 but in complexified z, \bar{z} coordinates.

Maps satisfying the Cauchy–Riemann equation $\bar{\partial}_z f = 0$, i.e. $z \mapsto z' = f(z)$, are conformal (angle-preserving). Their Jacobian is a diagonal matrix $\mathbf{D}f = \text{diag}[\partial_z f, \bar{\partial}_z f]$, combining rotation and scaling by the conformal factor $\lambda_{z|z'} = |\partial_z f|$. The subscript $z|z'$ indicates the map's source and target. Furthermore, for conformal maps,

$\Delta \log \lambda_{z|z'} = 4\partial_z \bar{\partial}_z \text{Re}[\log(\partial_z f)] = 0$. More generally, the magnitude and orientation of a map's shear is measured by the Beltrami coefficient $\mu_{z|z'} = \bar{\partial}_z f / \partial_z f$ which vanishes for a conformal map. Note that the Beltrami coefficients of the map f and of the quadratic form $(\mathbf{D}f)^\dagger \cdot \mathbf{D}f$ agree; $()^\dagger$ being the Hermitian adjoint. Geometrically, f maps infinitesimal circles to ellipses with eccentricity $|\mu_{z|z'}| / (1 - |\mu_{z|z'}|^2)^{1/2}$. If $|\mu_{z|z'}| < k < 1$ everywhere, f is called *quasi-conformal* (QC). In particular, QC maps preserve orientation. Notation-wise, their argument distinguishes QC maps $f(z, \bar{z})$ (also written $f(\mathbf{z})$), from conformal maps $f(z)$. In the following, we use the formalism of QC maps to develop our continuum theory (in Ref. [23], a similar QC approach was used to describe the growth of 2d tissues).

3. Isothermal coordinates

We now use the mathematics of QC maps to define a convenient parametrization of the tension triangulation. In 2d, a metric has 3 independent components, while an embedding map has two degrees of freedom. Thus, only a scalar degree of freedom remains. It is therefore always possible to find a set of *isothermal* coordinates [24] in which the metric is isotropic, characterized by a single scale factor. We begin by identifying isothermal coordinates $z(\xi, \bar{\xi})$ for the tension metric. Using Eq. (6), isotropy requires

$$4g_{\alpha\beta} d\xi^\alpha d\bar{\xi}^\beta = (\text{Tr} \sqrt{\mathbf{g}})^2 |d\xi + \mu_g d\bar{\xi}|^2 \quad (9)$$

$$\stackrel{!}{=} 2g_{z\bar{z}} dz d\bar{z} = g_{z\bar{z}} |\partial_\xi z d\xi + \bar{\partial}_{\bar{\xi}} z d\bar{\xi}|^2$$

where the Beltrami coefficient $\mu_g = g_{\xi\xi} / (\text{Tr}[\mathbf{g}] + 2\sqrt{\det \mathbf{g}})$ measures the anisotropy of \mathbf{g} . Therefore, $z(\xi, \bar{\xi})$ must fulfill a Beltrami equation:

$$\bar{\partial}_{\bar{\xi}} z(\xi, \bar{\xi}) = \mu_g \partial_\xi z(\xi, \bar{\xi}) \Leftrightarrow \mu_{\xi|z} = \mu_g \quad (10)$$

The QC map from Lagrangian ξ - to isothermal z -coordinates exactly removes the shear part of the metric. (By abuse of notation, we will denote both the coordinates and the map $\xi \mapsto z(\xi, \bar{\xi})$ by z). By the Measurable Riemann Mapping theorem [25], solutions to Eq. (10) exist as long as $|\mu_g| < k$ for some $k < 1$ (microscopically, the tension triangles must be uniformly non-degenerate). This fact will play a crucial role in guaranteeing the existence of mechanically stable states.

The metric thus becomes isotropic and is fully described by its conformal factor λ_g

$$g_{zz} = 0, g_{z\bar{z}} = 2\lambda_g^2(z, \bar{z}) \Leftrightarrow g_{\alpha\beta} = \lambda_g^2 \delta_{\alpha\beta} \quad (11)$$

Isothermal coordinates are conformal and do not distort angles (see Fig. 3; Appendix B 2 discusses the example of a hemisphere). The Liouville equation determines the Gaussian curvature of an isotropic metric:

$$K_g = -\lambda_g^{-2} \Delta \log \lambda_g \quad (12)$$

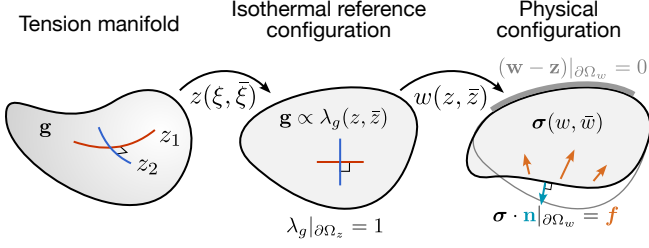


FIG. 3. Isothermal coordinates “flatten” the tension manifold without shear. We isothermally map to the “natural domain” defined by the boundary condition $\lambda_g|_{\partial\Omega} = 1$. The quasi-conformal map $w(z, \bar{z})$ maps the reference configuration to the physical domain. It determines the macroscopic stress tensor σ and is subject to physical boundary conditions (clamped boundary as gray shading, traction forces as red arrows).

where $\Delta = 4\partial_z\bar{\partial}_z$ is the Euclidean Laplacian. More generally, the St. Venant formula [26] gives the curvature of $g_{\alpha\beta} = \lambda_g^2(\delta_{\alpha\beta} + dg_{\alpha\beta})$ to linear order:

$$K_g = -\lambda_g^{-2}(\Delta \log \lambda_g + 2 \operatorname{Re}[\partial_z \bar{\partial}_z dg_{\bar{z}z} + \partial_z^2 dg_{zz}]) \quad (13)$$

Note that the composition of a solution to Eq. (10) with any conformal map yields another solution (indeed, for conformal maps, $\Delta \log \lambda_{z|z'} = 0$, so Eq. (12) is invariant). The BCs fix the conformal (“homogeneous”) solution. Throughout, we use “natural BCs”

$$\lambda_g(z, \bar{z})|_{\partial\Omega} = (\lambda_g(\xi, \bar{\xi})|\partial_\xi z)|_{\partial\Omega} = 1 \quad (14)$$

where $\partial\Omega$ is the system boundary. If \mathbf{g} is flat, this BC ensures $g_{z\bar{z}} = 2$, $\lambda_g = 1$ everywhere (Fig. 3).

B. Statics: Emergent elasticity

We introduced isothermal $z(\xi, \bar{\xi})$ as a convenient parametrization of the tension manifold. We now interpret $z(\xi, \bar{\xi})$ as a specific physical configuration, i.e. a map that places the Lagrangian material element ξ at physical position $\mathbf{r}(\xi) = \mathbf{z}(\xi)$ in the plane.

1. Emergent reference state

In the \mathbf{g} -isothermal configuration, the tensile stress becomes isotropic. Indeed, by Eq. (4):

$$\sigma_{zz} = 0, \quad \sigma_{z\bar{z}} = 2p_0\lambda_g(z, \bar{z}) \quad (15)$$

Therefore, with a pressure field

$$p = p_0\lambda_g(z, \bar{z}), \quad (16)$$

the macroscopic stress can be made to vanish identically: $\sigma_{\alpha\beta}^{\text{tot}} = \sigma_{\alpha\beta} - p\delta_{\alpha\beta} = 0$. The \mathbf{g} -isothermal configuration, thus, is a stress-free reference configuration

which *emerges* from a stress-only starting point. A liquid bubble raft provides a simple physical example (Appendix A). Surface tension balances against pressure so that the raft as a whole is stress-free (cutting it does not lead to macroscopic recoil). Equations (16) and (12) together imply a Laplace equation for the pressure in the stress-free configuration: $\Delta_z \log(p/p_0) = -K_g$.

In a physical configuration, the pressure field p is not an independent variable, but must obey the equation of state $p = P(n)$, Eq. (2). The stress-free reference state is physically attainable only if

$$p_0\lambda_g(\mathbf{z}) = P(n(\mathbf{z})). \quad (17)$$

For a flat tension metric, this relation reduces to $n(\mathbf{z}) = n(\xi) \det[\partial_\xi \mathbf{z}] = n_0$. If Eq. (17) is not fulfilled, the \mathbf{z} -configuration is not mechanically balanced. The tissue will adopt a different configuration with residual stresses that remain even when no traction is applied to the boundary [27]. Nonetheless, the isothermal \mathbf{z} -configuration will be a useful reference for the resulting general force-balanced states. In particular, it will be the starting point for linearizing the theory.

2. General force balanced states and conformal-isogonal decomposition

To relate the stress-free reference state $\mathbf{z}(\xi)$ to the realized physical state, we need to calculate how the macroscopic tensile stress σ changes when the system is deformed from the isothermal reference into a new configuration, $z \mapsto w(z, \bar{z})$. Physically, a deformation moves and reorients the local active force dipoles (cell interfaces), thereby modifying the macroscopic stress tensor. Mathematically, \mathbf{g} transforms according to Eq. (1). Using $g_{ab}(\mathbf{z}) = \lambda_g^2(\mathbf{z})\delta_{ab}$, Eq. (4) becomes:

$$[\sigma^2(\mathbf{w})]_{\alpha\beta} = p_0^2 \epsilon_{\alpha\gamma} g_{\gamma\delta}(\mathbf{w}) \epsilon_{\beta\delta} = p_0^2 \lambda_g^2(\mathbf{z}) \epsilon_{\alpha\gamma} \frac{\partial z_\kappa}{\partial w_\gamma} \frac{\partial z_\kappa}{\partial w_\delta} \epsilon_{\beta\delta}$$

The stress is thus determined by the square root of the Jacobian $\partial z_\alpha / \partial w_\beta$. In complexified notation:

$$\begin{bmatrix} \sigma_{\bar{w}w} & \sigma_{\bar{w}\bar{w}} \\ \sigma_{ww} & \sigma_{w\bar{w}} \end{bmatrix} = 2p_0\lambda_g \epsilon^T \cdot [\mathbf{D}w^\dagger \cdot \mathbf{D}w]^{-\frac{1}{2}} \cdot \epsilon \quad (18)$$

and the inverse Jacobian $(\mathbf{D}w)^{-1}$ reads

$$\mathbf{D}w^{-1} = \begin{bmatrix} \partial_w z & \bar{\partial}_w z \\ \partial_w \bar{z} & \bar{\partial}_w \bar{z} \end{bmatrix} = \begin{bmatrix} \partial_w z & 0 \\ 0 & \bar{\partial}_w \bar{z} \end{bmatrix} \cdot \begin{bmatrix} 1 & \mu_{w|z} \\ \bar{\mu}_{w|z} & 1 \end{bmatrix} \quad (19)$$

where $\mu_{w|z} = \bar{\partial}_w z / \partial_w z$ is the Beltrami coefficient $w(z, \bar{z})$. The μ -matrix factor is hermitian, which makes taking the square root in Eq (18) trivial. The resulting stress tensor components read

$$\sigma_{w\bar{w}} = 2p_0\lambda_g|\partial_w z|, \quad \sigma_{ww} = -2p_0\lambda_g|\partial_w z|\mu_{w|z} \quad (20)$$

Eq. (20) relates spatial deformation to the changes in physical stress, and can be interpreted as an emergent stress-strain relationship [22]. The anisotropic strain relative to the isothermal reference state sets the deviatoric stress σ_{ww} . Crucially, the stress anisotropy is *not* identical to the “microscopic” tension anisotropy (differences in interface tensions τ_{ij} , or, geometrically, anisotropy of tension triangles). We will return to this important distinction in Sect. D where we define a tension anisotropy field in the continuum.

In Cartesian notation, the matrix square-root Eq. (18) can be evaluated via the singular value decomposition of $\mathbf{D}w = U \cdot \Lambda \cdot V^T$:

$$\boldsymbol{\sigma}(\mathbf{w}) = p_0 \lambda_g \frac{U \cdot \Lambda \cdot U^T}{\det \Lambda} \quad (21)$$

In the companion paper [18], we derive the stress-metric relation in the form of Eq. (21) by explicit coarse graining.

In mechanical balance, the divergence of the tensile stress must be compensated by a pressure gradient. In complexified notation, force balance Eq. (5) reads

$$\bar{\partial}_w \sigma_{\bar{w}w} + \partial_w \sigma_{ww} = 2\bar{\partial}_w p \quad (22a)$$

$$\Rightarrow \partial_w \bar{\partial}_w \sigma_{\bar{w}w} + \partial_w^2 \sigma_{ww} = 2\partial_w \bar{\partial}_w p \quad (22b)$$

The RHS is real – the net tensile force must be curl-free. This entails a solvability condition:

$$\text{Im}[\partial_w^2 \sigma_{ww}] = \text{Im}\left[\partial_w^2 \left(\lambda_g \frac{|\partial_w z|}{\partial_w z} \bar{\partial}_w z\right)\right] = 0. \quad (23)$$

For a flat tension metric ($K_g = 0$, so $\lambda_g = 1$) and small displacement $|w - z| \ll 1$, this condition can be simplified. In Cartesian coordinates:

$$\Delta(\epsilon_{\alpha\beta} \partial_\beta w_\alpha(\mathbf{z})) = 0 \quad (24)$$

The curl of the deformation w must be harmonic. Equation (23) constrains force-balanced physical configurations $w(z, \bar{z})$. Two classes of solutions are readily apparent.

Conformal deformations. First, conformal maps $z = f(w)$, for which $\partial_w \bar{z} = \bar{\partial}_w z = 0$, so Eq. (23) holds trivially. Under conformal maps, σ remains isotropic, while the pressure required for force balance is $p \mapsto p/\lambda_{z|w}$. This allows broadening the conditions under which a stress-free configuration exists. If the reference state $\mathbf{z}(\boldsymbol{\xi})$ fails to respect $n(\mathbf{z}) = n_0$ (Eq. (17)), we can find a conformal map $w(z)$ so that $n(\mathbf{w}) = \lambda_{z|w}^{-2} n(\mathbf{z}) = n_0$, provided $\Delta \log n(\mathbf{z}) = 0$ (the restriction is due to $\Delta \log \lambda_{z|w} = 0$).

As an aside, we note that the relation $p = p_0/\lambda_{z|w}$ between conformal deformations, which curve line elements, and pressure gradients can be understood as a continuum manifestation of the Young–Laplace law [12]. Consider a straight line with normal \mathbf{n} in the reference configuration (z -coordinates). Through a conformal deformation it acquires a curvature $1/R = \mathbf{n} \cdot (2\bar{\partial}_w |\partial_w z|)$ (Appendix C), while the pressure drop dp across the line

element changes to $p_0 \mathbf{n} \cdot (2\bar{\partial}_w |\partial_w z|) dr$. Recall that in \mathbf{g} -isothermal coordinates, $p_0 dr = d\tau$ is the effective line tension, so that $d\tau/R = dp$ – a differential form of the Young–Laplace law.

Isogonal deformations. Second, for $\lambda_g = 1$, a map $z(w, \bar{w}) = \bar{\partial}_w \theta$ defined by the gradient of a real potential θ is a solution since

$$\text{Im}\left[\partial_w^2 \left(\frac{|\partial_w z|}{\partial_w z} \bar{\partial}_w z\right)\right] = \text{Im}[\partial_w^2 \bar{\partial}_w^2 \theta] = 0 \quad (25)$$

In contrast to conformal maps, potential gradients generically create anisotropic stress. Indeed, by Eq. (20), θ is the Airy function of the resulting stress:

$$\sigma_{w\bar{w}} = -2p_0 \partial_w \bar{\partial}_w \theta, \quad \sigma_{ww} = 2p_0 \bar{\partial}_w^2 \theta \quad (26)$$

An analogous, if lengthy, calculation shows that for $K_g \neq 0$, $z = \lambda_g^{-2} \bar{\partial}_w \theta$ is a perturbative solution to Eq. (23) (it corresponds to the Riemannian gradient of θ with respect to \mathbf{g}). The manifold of force-balanced states parametrized by θ corresponds to the *isogonal* “breathing” modes of the discrete ATN model [10], and we will therefore refer to θ as the isogonal potential (in the mathematical literature, such a potential defines a “weighted triangulation” [28]). Conformal displacements also have an exact equivalent at the cell-level – a certain “local” Möbius symmetry of force-balanced tilings. The discrete-continuum connections are detailed in the companion paper [18]. Conformal and isogonal displacements exhaust all solutions to Eq. (23) (Appendix D). Any physical configuration w can hence be obtained from the reference z by composing a potential map and a conformal map. The two modes suffice to accommodate arbitrary deformations imposed on the system boundary (Appendix E).

In summary, starting from Lagrangian labels ξ , we mapped first to the \mathbf{g} -isothermal reference configuration z , and then to the physical configuration w :

$$\xi \xrightarrow{\mathbf{g}\text{-isothermal}} z(\xi, \bar{\xi}) \xrightarrow{\text{force balance}} w(z, \bar{z}). \quad (27)$$

Appendix B1 provides an elementary example of this mapping. While force balance in the bulk imposes a conformal–isogonal structure on the deformation w , BCs and a specific constitutive relation for pressure are required to determine the physical configuration completely.

3. Fully compressible cells

By Eq. (23), for all isogonal–conformal configurations, there is a pressure field that brings the system into mechanical equilibrium. However, physically, the pressure field must also obey the equation of state $P(n)$, which we impose now.

Let us first discuss a specific case, the continuum equivalent to the “classic ATN” setting investigated in [10]. For a flat tension metric \mathbf{g} , Eq. 16 implies a constant pressure $p = p_0$. In the bulk, tensions are in force balance

“on their own”: only at the boundary, a pressure drop p_0 is required for normal force balance. This state can be realized by freely compressible cells with an “equation of state” $p = p_0$ (i.e., cells can freely exchange volume with one another, and p_0 acts as a Lagrange multiplier for the total tissue area).

Purely isogonal deformations of the reference state do not require pressure gradients, since the tensile stress is balanced on its own:

$$\bar{\partial}_w \sigma_{w\bar{w}} + \partial_w \sigma_{ww} = 2p_0 [\bar{\partial}_w (\partial_w \bar{\partial}_w \theta) - \partial_w (\bar{\partial}_w^2 \theta)] = 0 \quad (28)$$

Since the equation of state is trivial, $P(n) = p_0$, pressure also remains invariant. Isogonal modes in the bulk are therefore true zero-energy modes.

Under conformal deformations $w(z)$, however, the tensile stress $\sigma_{w\bar{w}} = 2p_0 |\partial_w z|$ becomes non-uniform, implying pressure gradients. To sustain such pressure gradients, a finite compressibility (a non-constant $P(n)$) is required. Now, force balance $\partial_\beta p = \partial_\alpha \sigma_{\alpha\beta}$ selects a single physical solution among the isogonal–conformal family of solutions by fixing the isogonal potential θ in the bulk. Mechanical BCs further fix the boundary DOFs of the conformal and isogonal maps.

4. Linearized theory: effective Cauchy elasticity

To understand the physics resulting from the interplay of conformal–isogonal structure and the constitutive law for pressure, we now expand stress and pressure for small deformations $w = z + u(z, \bar{z})$, $|\partial_z u| \ll 1$ around the isothermal, stress-free reference state. We further assume small cell-density gradients in the reference state, $n(z, \bar{z}) = n_0(1 + \delta n(z, \bar{z}))$, and small curvature K_g (hence, $\log \lambda_g$ is also small). In the discrete setting, cell areas are close to the Voronoi areas of the tension triangulation.

Near the reference cell density n_0 , one can linearize the equation of state $P(n) \approx p_0(1 + B(n/n_0 - 1))$, where B is the non-dimensionalized cellular bulk modulus. Evaluating at $n(w, \bar{w})$, one obtains

$$p(w, \bar{w}) = p_0 \{1 - B(\text{Re}[\partial_z u] + \delta n)\} \quad (29)$$

Also expanding the tensile stress Eq. (20) to linear order in u , the total stress becomes

$$\begin{aligned} \sigma_{w\bar{w}}^{\text{tot}} &= 2p_0 \{ (2B - 1) \text{Re}[\partial_z u] + \log \lambda_g - 2B\delta n \} \\ \sigma_{ww}^{\text{tot}} &= 2p_0 \partial_z \bar{u} \end{aligned} \quad (30)$$

In Cartesian notation, one finds

$$\begin{aligned} \sigma_{\gamma\gamma}^{\text{tot}} &= 2p_0 \left(B - \frac{1}{2} \right) \partial_\gamma u_\gamma + 2p_0 (\log \lambda_g + B\delta n) \\ \sigma_{\alpha\beta}^{\text{tot}} - \frac{1}{2} \delta_{\alpha\beta} \sigma_{\gamma\gamma}^{\text{tot}} &= \frac{p_0}{2} (\partial_\alpha u_\beta + \partial_\beta u_\alpha - \delta_{\alpha\beta} \partial_\gamma u_\gamma) \end{aligned} \quad (31)$$

Existence and stability of force-balanced states. Eq. (31) is mathematically equivalent to linear isotropic elasticity [3] with an isotropic “body force” $p_0 \partial_\beta (\log \lambda_g +$

$B\delta n)$. However, the underlying physical picture is quite different: a conventional elastic material is akin to a Hookean spring, where strain relative to the rest length triggers a restoring force. In an active solid, active force dipoles, whose tension is independent of elastic strain, must be arranged (embedded) to balance against the isotropic pressure. The map to linear elasticity shows that a force-balanced embedding exists for any active tension configuration \mathbf{g} . This result relies on the existence of isothermal coordinates $z(\xi, \bar{\xi})$, in which the tensile stress is isotropic, and of two compatible modes (isogonal and conformal), which can accommodate elastic deformations in response to external and body forces.

One identifies the effective shear and bulk moduli as $\frac{1}{2}p_0$ and $(B - 1/2)p_0$. At higher orders in the gradient expansion, the elastic moduli scale like $\sim p$ and thus become non-uniform (high-pressure regions are stiffer). The finite shear modulus indicates that active tension networks are effective solids, rather than fluids. Furthermore, for a sufficiently large cellular bulk modulus B , both effective moduli are positive. The constitutive relation $P(n)$ thus ensures that the mechanical equilibrium is stable. If pressures are instead upgraded to independent, active degrees of freedom (like the tensions τ_{ij}), mechanical stability is no longer guaranteed. For example, fixing both pressure and surface tension in a soap bubble renders it unstable.

Biharmonic equation and effective Airy function. By Eq. (31), force balance $\partial_\alpha \sigma_{\alpha\beta}^{\text{tot}} = 0$ becomes:

$$\Delta u_\beta + (2B - 1) \partial_\beta (\partial_\alpha u_\alpha) = -2\partial_\beta (B\delta n + \log \lambda_g) \quad (32)$$

As expected from the solvability analysis above, the general solution to Eq. (32) can be written as $u_\alpha = \partial_\alpha \theta + \nu_\alpha$ where ν_α is a conformal vector field [26, 29]. Equation (32) reduces to:

$$\Delta \theta = -(1 - (2B)^{-1}) \partial_\alpha \nu_\alpha - \delta n - B^{-1} \log \lambda_g + C \quad (33)$$

where C is an integration constant which can be absorbed into a uniform scaling. Using Eq. (33) and the Cauchy–Riemann equations for ν_α , the stress reads:

$$\sigma_{\alpha\beta}^{\text{tot}} = p_0 (\partial_\alpha \partial_\beta \theta - \Delta^2 \theta \delta_{\alpha\beta}) = -p_0 \epsilon_{\alpha\gamma} \epsilon_{\beta\delta} \partial_\gamma \partial_\delta \theta \quad (34)$$

Note that Eq. (34) is valid only in a force-balanced state, i.e. when Eq. (33) holds. For an arbitrary, unbalanced deformation u_α , one must use Eq. (31).

Hence, the isogonal potential θ is identical to the Airy stress function [30]. Due to Eqs. (12) and (33), θ obeys a biharmonic equation analogous to classical elasticity:

$$\Delta^2 \theta = \Delta \delta n - B^{-1} K_g \quad (35)$$

Gaussian curvature of the tension metric and δn appear as source terms, implying residual stresses even for traction-free BCs. These stresses result from an incompatibility between a constant cell density and an isotropic tensile stress (the macroscopically stress-free state does not have uniform pressure). The biharmonic equation

Eq. (35), together with BCs on stress $\sigma_{\alpha\beta}$ or displacement u_α , fully determines the tissue shape. It can be solved numerically or via complex variable techniques (referred to as Kolosov-Muskhelishvili formalism) [26]. Appendix B presents two worked examples.

Up to the overall scale p_0 , the only free parameter of the theory is the cellular bulk modulus B . Let us briefly discuss four special cases: (i) For incompressible cells, $B \rightarrow \infty$ forcing $\partial_\alpha u_\alpha = -\delta n$. (ii) If pressures follow the ideal gas law $p(n)p_0 n/n_0$, i.e. $B = 1$, the *total* bulk and shear moduli are equal, which may be relevant to experiments on conventional foams with air-filled bubbles. (iii) For $B = 1/2$, the total bulk modulus vanishes, so that the conformal mode f_α becomes soft. If $B < 1/2$, the total bulk modulus is negative: intracellular pressure is insufficient to balance the isotropic tensile stress. Mechanical stability then requires a constraint on the total area. (iv) For fully compressible cells $B = 0$, the isogonal potential θ is an unconstrained soft mode. However, conformal modes, which require pressure gradients, cannot be accommodated. By Eq. (35), freely compressible cells (i.e., $B = 0$) are unstable if $K_g \neq 0$.

In summary, boundary forces deform the tissue away from the emergent reference state $z(\xi, \bar{\xi})$. Incompatible cell densities and tension curvature lead to residual stresses, present even for free boundaries. The physical stress is governed by effective linear elasticity. The biharmonic Eq. (35) for the isogonal potential (the effective Airy function) implies that the physical configuration minimizes the physical stress, under the constraints imposed by BCs [31]. A remarkable consequence of these results is that the shape and macroscopic mechanical properties of the tissue are determined by the tension metric and cell density alone. There are many microscopic tension configurations (tension triangulations) that have the same \mathbf{g} and n . On a macroscopic level, they are all equivalent – the microscopic details are irrelevant for the static problem.

C. Active tension dynamics: Quasiconformal flow

We have seen how the cell positions $\xi \mapsto w(\xi, \bar{\xi})$ embed the tension metric into physical space, and how they are determined by force balance. We next consider the dynamics of the embedding $w(\xi, \bar{\xi}, t)$ in response to changes in active tension $\partial_t \mathbf{g}$. These dynamics are subject to biological control, which involves genetic programs and mechanochemical feedback loops [32–35]. In the following, we do not assume any specific form, and instead consider a general active tension dynamics defined by

$$\partial_t \log \mathbf{g}(\boldsymbol{\xi}, t) = \mathbf{m}(\boldsymbol{\xi}, t, \boldsymbol{\sigma}, \dots) \quad (36)$$

The rate-of-change tensor \mathbf{m} will act as an effective forcing term that internally drives the morphing of the active solid from one shape to another.

1. Adiabatic approximation

We will assume rapid relaxation towards mechanical equilibrium. Consider relaxation dynamics of the cell positions \mathbf{r}

$$\Gamma^{-1} \partial_t r_\alpha(\xi, \bar{\xi}, t) = \partial_\alpha \sigma_{\alpha\beta}(t) - \partial_\beta p(t) \quad (37)$$

where Γ is a friction coefficient. The stress σ depends both on $\mathbf{r}(t)$ and $\mathbf{g}(t)$ by Eq. (4), and is thus time-dependent. The timescale of relaxation to equilibrium is given by $L\Gamma/p_0$, where L is the system length scale. In the limit where relaxation is rapid (compared to tension dynamics $\partial_t \log \mathbf{g}$), Eq. (37) reduces to force balance:

$$\partial_\alpha \sigma_{\alpha\beta}(t) - \partial_\beta p(t) \approx 0 \quad (38)$$

Due to rapid relaxation, transient friction or viscous stress will play no important role. The cells, therefore, adopt the instantaneous equilibrium configuration $\mathbf{w}[\mathbf{g}(t)](\xi, \bar{\xi})$, considered as a functional of the time-dependent tension metric $\mathbf{g}(t)$.

In the adiabatic approximation, the tissue flow due to tension dynamics can be computed by the chain rule:

$$\begin{aligned} \partial_t w[\mathbf{g}(t)](\xi, \bar{\xi}) &= \frac{\delta w[\mathbf{g}]}{\delta \mathbf{g}} \circ \partial_t \mathbf{g} = \frac{\delta w[\mathbf{g}]}{\delta \mathbf{g}} \circ \mathbf{m}(\xi, \bar{\xi}) \\ &:= \int \frac{\delta w[\mathbf{g}](\xi, \bar{\xi})}{\delta \mathbf{g}(\xi', \bar{\xi}')} \mathbf{m}(\xi', \bar{\xi}') d\xi' d\bar{\xi}' \end{aligned} \quad (39)$$

The functional derivative $\delta w/\delta \mathbf{g}$ is a convolutional integral, defined on the second line. The adiabatic flow is thus “non-local”: a local change in contractility induces strain across the tissue. We evaluate Eq. (39) by the composition of incremental maps and further decompose $w(\xi, \bar{\xi})$ into $\xi \mapsto z(\xi, \bar{\xi}) \mapsto w(z, \bar{z})$, from ξ to the reference z , and from z to the physical state. By the chain rule:

$$\frac{\delta w[\mathbf{g}](\xi, \bar{\xi})}{\delta \mathbf{g}} = \frac{\delta w[\mathbf{g}]}{\delta z} \circ \frac{\delta z[\mathbf{g}]}{\delta \mathbf{g}} + \frac{\delta w[\mathbf{g}]}{\delta \bar{z}} \circ \frac{\delta \bar{z}[\mathbf{g}]}{\delta \mathbf{g}} \quad (40)$$

Here, $\delta z/\delta \mathbf{g}$ describes the variation of the isothermal embedding of \mathbf{g} , while $\delta w/\delta z$ involves solving an elasticity problem, under the constraints imposed by the physical BCs (e.g., zero normal stress).

2. Adiabatic flow of the reference configuration

The dynamics of $z(\xi, \bar{\xi}, t)$ is given by the Beltrami Eq. (10). Consider an infinitesimal increment

$$\mathbf{g}(\boldsymbol{\xi}, t) \mapsto \mathbf{g}(\boldsymbol{\xi}, t) + (\partial_t \mathbf{g}(\boldsymbol{\xi}, t)) dt \quad (41)$$

The resulting flow $z \mapsto z + \dot{z} dt$ must reestablish a state of isotropic stress. Rather than in Lagrangian ξ -coordinates, we express the adiabatic flow in the current $z(t)$ coordinates, so that $\dot{z}(z(t), z(t), t)$ is the Eulerian

velocity field. For brevity, we write $z = z(t)$. Expanding the Beltrami Eq. (10) in dt , and using the definition Eq. (36) of the \mathbf{m} -tensor leads to the simple expression

$$\bar{\partial}_z \dot{z}(z, \bar{z}) = \frac{1}{4} m_{zz}(z, \bar{z}, t), \quad \text{Re}[\bar{\partial}_z \dot{z}]|_{\partial\Omega} = m_{z\bar{z}}|_{\partial\Omega} \quad (42)$$

Eq. (42) defines a sequence of infinitesimal QC deformations – a QC flow (also called a Beltrami flow). The QC flow equation is linear and can be solved by the method of Green’s functions, even for large deformations [25] (Appendix F). Eq. (42) describes how an anisotropic *change* of active tension induces a corresponding shear deformation of the isothermal reference state.

For free boundaries (and under an additional condition explained below), flow of the reference state z translates directly into flow of the physical configuration w . Eq. (42) can be brought into a more familiar form by applying ∂_z and changing to Cartesian notation

$$\Delta(\dot{z})_\beta = \partial_\alpha (m_{\alpha\beta} - \frac{1}{2} m_{\gamma\gamma} \delta_{\alpha\beta}) \quad (43)$$

Eq. (43) resembles a Stokes flow, driven by the divergence \mathbf{m} . Recall, however, that \mathbf{m} is not an active stress but rather the *rate of change* of the tension metric. In the adiabatic regime, the system follows the force-balanced configuration imposed by the internal tension configuration. The flow rate is thus set by the timescale on which cells regulate contractility, and not by the (rapid) rate Γ of mechanical relaxation. Adiabatic flow is not stress relaxation: In the z -configuration, the total macroscopic stress $\boldsymbol{\sigma}^{\text{tot}} = 0$ throughout the adiabatic QC flow.

3. Adiabatic flow of the physical configuration

We are ultimately interested in the dynamics of the physical configuration w , which may differ from z due to external or body forces. The change of the map from reference to physical configuration is $w(z, \bar{z}, t + dt) = w(z, \bar{z}, t) + \dot{w}(z, \bar{z}, t) dt$. The physical flow \dot{w} is determined by the BCs and the constitutive relation $P(n)$ (see Sect. B 4). For instance, for $B = \infty$, one obtains:

$$\text{Re}[\partial_z \dot{w}] = 0 \quad (44a)$$

$$\partial_z \bar{\partial}_z \text{Im}[\partial_z (\dot{z} - \dot{w})] = 0 \quad (44b)$$

Eq. (44a) enforces incompressibility. Eq. (44b) derives from the solvability Eq. (23), expanded for $|w - z| \ll 1, |\lambda_g - 1| \ll 1$: the physical flow *relative* to the changing reference configuration must obey the force-balance compatibility condition. For free BCs, Eq. (44b) could be solved simply by $\dot{w} = \dot{z}$. By Eq. (44a), this requires \dot{z} to be incompressible, i.e., $\dot{z} = 2i\bar{\partial}_z \psi$ for a real-valued solenoidal potential ψ . Plugging $\dot{z} = 2i\bar{\partial}_z \psi$ into Eq. (42), Eq. (13) leads to the condition $\dot{K}_g = 0$. Hence, for flat changes in \mathbf{g} and free BCs, reference-flow translates directly into physical flow. In general, one must solve the elasticity problem Eq. (44) to determine w in terms of z .

Together, Eqs. (42) and (44) describe the reestablishment of force balance after a change of stress. At this point, it would appear that a large shape change requires building up increasing tension anisotropy (i.e., tension triangles anisotropy). As we will see next, however, cell rearrangements plastically lock in past tension dynamics while resetting the built-up tension anisotropy. Macroscopically, these dynamics appear as a steady plastic flow.

D. Topological rearrangement

1. Continuum representation of microscale topology and tension anisotropy

Large tissue deformations cause cells to rearrange, leading to plastic shape changes. In the discrete model, such T1 processes correspond to edge flips that change the adjacency graph of the triangulation (Fig. 4). (“T1” stands for “topological 1”; in the following, we use “topology” to refer to the adjacency graph and not the gross topology of the tension manifold, which we assume to be that of a disk). These flips occur when the length of a cell-cell interface vanishes $\ell_{ij} = 0$ and do not manifest themselves in the tension metric. The challenge is to represent the inherently discrete T1 processes in the continuum. We now introduce a mathematical framework to do so and return to the physical consequences of T1s for plastic flow in Sects. D 3–D 4.

Let us recall that in addition to the tension metric \mathbf{g} , the discrete ATN model depends on the topology of the cell tiling, i.e., the vertex adjacency matrix. To capture the adjacency information in the continuum, we introduce an “adjacency metric” $a_{\alpha\beta}(\boldsymbol{\xi})$ defined so that adjacent cells have unit distance. It is the continuum limit of a triangulation with the same adjacency as the tension triangulation, but with all edge lengths set to unity. Thus $\mathbf{g}(\boldsymbol{\xi})$ and $\mathbf{a}(\boldsymbol{\xi})$ define two distinct metrics on the same manifold. The Lagrangian coordinates $\boldsymbol{\xi}$ are attached to material elements (e.g. cells) and label corresponding points. The adjacency metric “geometrizes” the topological information on cell-cell adjacency, and is closely related to the Koebe-Andreev-Thurston circle packing theorem (see Discussion).

Intuitively, the “discrepancy” between \mathbf{a} and \mathbf{g} measures the shape of tension triangles in the continuum theory, notably, the local tension anisotropy (\mathbf{a} is made from equilateral “adjacency” triangles, \mathbf{g} from potentially anisotropic tension triangles). Gaussian curvature of \mathbf{a} corresponds to the net density of topological defects in a triangular lattice (i.e., 5- or 7-sided cells, Fig. 4) [36]. The area element of \mathbf{a} defines the local cell density, $n = n_0 \sqrt{\det \mathbf{a}}$ (we dimensionalize $\mathbf{a} \mapsto \mathbf{a}/n_0$ so that \mathbf{a} has units of [length]²) [37].

Together, \mathbf{a} and \mathbf{g} furnish a complete continuum description of the cell tiling and its mechanics. The ability to control tensions and topology separately is what separates the ATN model from an ordinary fluid foam, where

$\mathbf{g} = \mathbf{a}$ (all tensions are equal and can be set to unity).

Cell rearrangements correspond to dynamics in the adjacency metric \mathbf{a} . To describe them, we now introduce isothermal coordinates $\zeta(\xi, \bar{\xi})$ for the adjacency metric \mathbf{a} , analogous to the \mathbf{g} -isothermal coordinates z :

$$\bar{\partial}_\xi \zeta = \mu_a \partial_\xi \zeta \Rightarrow a_{\zeta\zeta} = 0, \quad a_{\zeta\bar{\zeta}} = 2\lambda_a^2 \quad (45)$$

The common Lagrangian cell labels ξ establish a one-to-one correspondence between the two isothermal coordinates z, ζ for the tension and adjacency metric:

$$\begin{array}{ccc} & z(\xi, \bar{\xi}) & \xrightarrow{\mu_{z|w}} w(z, \bar{z}) \\ \mathbf{g}\text{-iso} \nearrow & \uparrow \mu_{\zeta|z} & \nearrow \\ \xi & & \\ \mathbf{a}\text{-iso} \searrow & \zeta(\xi, \bar{\xi}) & \xrightarrow{\mu_{\zeta|w}} \end{array} \quad (46)$$

Since \mathbf{a} and \mathbf{g} are independent metrics, $\zeta(\xi, \bar{\xi})$ and $z(\xi, \bar{\xi})$ are independent maps. Via Eq. (46), we switch from the ξ - to the ζ -basis:

$$\xi \xrightarrow{\mathbf{a}\text{-iso}} \zeta(\xi, \bar{\xi}) \xrightarrow{\mathbf{g}\text{-iso}} z(\zeta, \bar{\zeta}) \xrightarrow{\partial_\alpha \sigma_{\alpha\beta} = \partial_\beta p} w(z, \bar{z}) \quad (47)$$

The adjacency coordinates ζ serve as a convenient set of coordinates adapted to the adjacency of the cell network – in ζ -coordinates, cells have isotropic shapes and density $n_0 \lambda_a^2$. If interfacial tensions are perfectly isotropic, $\mathbf{a} = \mathbf{g}$ and $z = \zeta$. More generally, the Jacobian $\mathbf{D}z(\zeta, \bar{\zeta})$ of the QC map from ζ to the tension reference state z defines the local tension configuration [19, 38]. Microscopically, $\mathbf{D}z(\zeta, \bar{\zeta})$ deforms equilateral “adjacency” triangles into anisotropic tension triangles. In particular, the Beltrami coefficient $\mu_{\zeta|z} = \bar{\partial}_\zeta z / \partial_\zeta z = \mu_g(\zeta, \bar{\zeta})$ encodes the magnitude and direction of the tension anisotropy. Overall, in z -coordinates, the adjacent metric specifies the local cell density and the tension anisotropy.

By contrast, the map from z to the physical configuration w , and its Beltrami coefficient $\mu_{z|w} = \bar{\partial}_z w / \partial_z w$, determines the elastic shear and macroscopic deviatoric stress. In fact, $\mu_{z|w}$ is proportional to deviatoric stress [cf. Eq. (20)]. The total anisotropy of the map $w(\zeta, \bar{\zeta})$ from isotropic adjacency triangles to the physical configuration is given by the chain rule:

$$\begin{aligned} \mu_{\zeta|w} &= \frac{\bar{\partial}_\zeta w}{\partial_\zeta w} = \frac{\bar{\partial}_\zeta z \partial_z w + \bar{\partial}_\zeta \bar{z} \bar{\partial}_z w}{\partial_\zeta z \partial_z w + \partial_\zeta \bar{z} \bar{\partial}_z w} \\ &= \frac{\mu_{\zeta|z} + e^{-i2\phi_{\zeta|z}} \mu_{z|w}}{1 + e^{-i2\phi_{\zeta|z}} \bar{\mu}_{\zeta|z} \mu_{z|w}} \approx \mu_{\zeta|z} + e^{-i2\phi_{\zeta|z}} \mu_{z|w} \end{aligned} \quad (48)$$

where $e^{-i2\phi_{\zeta|z}} = \bar{\partial}_\zeta z / \partial_\zeta z$, and we assumed $|\mu_{\zeta|z}|, |\mu_{z|w}| \ll 1$ in the last step.

Taken together, the \mathbf{a} -isothermal coordinates ζ allow us to define the local tension configuration in the continuum as the Jacobian of the map $z(\zeta)$. Per Sect. B, the macroscopic stress is *independent* of the adjacency metric and hence of tension anisotropy $\mu_{\zeta|z}$. However, the latter plays an important role in cell rearrangement, as we will see below.

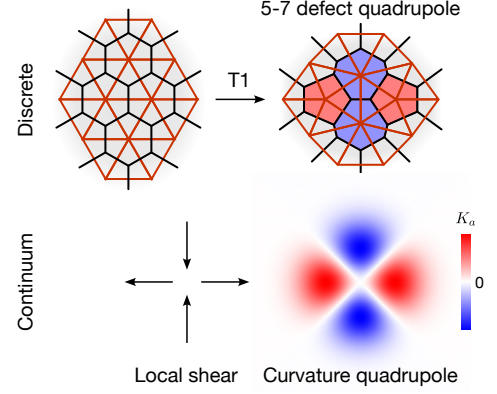


FIG. 4. In an hexagonal lattice, a T1 transition generates two 5-7 defect pairs. Correspondingly, a localized shear generates a curvature quadrupole in the adjacency metric \mathbf{a} .

2. Kinematics of cell rearrangement: Flip flow

Dynamics of the adjacency metric are driven by the (oriented) T1 rate $R(\xi, \bar{\xi}, t)$, to which individual T1s make infinitesimal contributions. These increments are most easily expressed in Eulerian $\zeta(t)$ -coordinates

$$\mathbf{a}(\zeta(t), t) \mapsto \mathbf{a}(\zeta(t), t) + \partial_t \mathbf{a}(\zeta(t), t) dt \quad (49)$$

As above, we write $\zeta = \zeta(t)$ for short in the following. Since T1s do not change the cell number, they correspond to pure shear deformation of \mathbf{a} :

$$\partial_t \lambda_a(\zeta, \bar{\zeta}, t) = 0, \quad \partial_t \mu_a(\zeta, \bar{\zeta}, t) := R(\zeta, \bar{\zeta}, t) \quad (50)$$

In the present framework, Eq. (50) is the definition of the rate of topological rearrangement in the continuum. We introduced R as a complex Beltrami coefficient; it can also be represented by a (trace-free) Cartesian tensor \mathbf{R} analogous to \mathbf{m} in Eq. (36).

For example, consider a localized “rearrangement event” $da_{\zeta\zeta} = \lambda_a^2 R dt = c \ell_R^2 e^{-\zeta\bar{\zeta}/(2\ell_R^2)} dt$ with spatial extent ℓ_R , on an initially uniform background $\lambda_a = 1$. The complex coefficient c sets the shear orientation and magnitude. To mimic an “isolated T1” in a hexagonal lattice, one sets ℓ_R to the scale of the cell size, and $|c| \sim 1/t_{T1}$, where t_{T1} is the timescale of the T1 process. Microscopically, such a T1 creates a 5-7 defect pair (Fig. 4, top). In the continuum, defects are localized quadrupoles in the adjacency curvature K_a . Indeed, using the St. Venant formula Eq. (13), the increment $da_{\zeta\zeta}$ leads to:

$$dK_a = \ell_R^{-2} \text{Re}[c\bar{z}^2] e^{-\zeta\bar{\zeta}/(2\ell_R^2)} dt \quad (51)$$

For $\arg c = 0$, $dK_a \propto (\zeta_1^2 - \zeta_2^2) dt$ (Fig. 4, bottom).

The T1-induced shear deformation Eq. (50) requires an update to the isothermal ζ -coordinates, $\zeta(t) \mapsto \zeta(t + dt) = \zeta(t) + \dot{\zeta}(\zeta(t), \bar{\zeta}(t), t) dt$. We refer to $\dot{\zeta}(t)$ as the *flip flow*, since it corresponds to edge flips in the discrete triangulation. The flip flow is quasi-conformal and obeys:

$$\bar{\partial}_\zeta \dot{\zeta}(\zeta, \bar{\zeta}, t) = \partial_t \mu_a(\zeta, \bar{\zeta}, t) = R(\zeta, \bar{\zeta}, t) \quad (52)$$

The time derivative of $\mathbf{g}(\zeta)$ combines intrinsic active tension dynamics m and cell rearrangement R . The former leads to reference state flow $z \mapsto z + \dot{z} dt$, and the latter to the coordinate transformation $\zeta \mapsto \zeta + \dot{\zeta} dt$. The flip flow thus enters as a continuous “reparametrization” of the tension manifold. The dynamics of the Beltrami-coefficient $\mu_{\zeta|z}$, assuming $|\mu_{\zeta|z}| \ll 1$, is given by:

$$\frac{d}{dt}\mu_{\zeta|z} - \left(\text{Re}[\dot{\zeta}\partial_{\zeta}]\mu_{\zeta|z} + i2\mu_z \text{Im}[\partial_{\zeta}\dot{\zeta}] \right) \approx \partial_t\mu_g(\zeta, \bar{\zeta}) - \partial_t\mu_a(\zeta, \bar{\zeta}) \quad (53)$$

The bracketed terms on the LHS represent advection and co-rotation and will be suppressed in the following. The RHS arises from the QC transformations of z and ζ (see Appendix G 1 for the derivation; Fig. 8 illustrates the underlying geometry.).

In summary, T1s change the adjacency metric \mathbf{a} , which we represent via the flip flow $\dot{\zeta}$. The flip flow is a reparameterization that changes the tension anisotropy, but has no *instantaneous* effect on the tension metric $\mathbf{g}(\xi)$ in fixed, Lagrangian coordinates. In our framework, cell rearrangement is thus a purely kinematic process. This is best motivated by looking at physical space. Microscopically, a T1 flips an edge whose physical length $\ell_{ij} = 0$, and is hence “invisible”: it has no instantaneous effect on physical shape or macroscopic stress. We next describe a specific model for the *dynamic* change of the tension manifold elicited by the *kinematic* effect of T1s on tension anisotropy.

3. Dynamics of cell rearrangement: Active and passive T1s

To fill the kinematic relations (52)–(53) with life, we need to specify a continuum law for the rate and orientation of T1s R and a prescription for the dynamics of \mathbf{g} caused by rearrangements.

As a minimal, phenomenological model for topological plasticity, we propose to represent T1s by continuous relaxation of the total anisotropy $\mu_{\zeta|w}$. The (oriented) rearrangement rate, therefore, reads

$$R(\zeta, \bar{\zeta}) = -\gamma_{\text{T1}} \frac{\delta|\mu_{\zeta|w}|^2}{\delta\bar{\mu}_a} = \gamma_{\text{T1}}\mu_{\zeta|w} \quad (54)$$

Here, γ_{T1} is a rate coefficient (the “T1 rate”), which depends on the distribution of microscopic tension configurations, as we discuss below. The variation of $|\mu_{\zeta|w}|^2$ follows from the Beltrami composition formula (48) (see Appendix G 2). The total anisotropy decomposes into the tension anisotropy and the stress anisotropy

$$\mu_{\zeta|w} \approx \mu_{\zeta|z} + e^{-i2\phi_{\zeta|z}}\mu_{z|w}. \quad (55)$$

T1s can thus be driven by internal tension changes or by elastic deformations due to external forces [19, 38]. Accordingly, we define active and passive T1 rates

$$R_{\text{act}} = \gamma_{\text{T1}}\mu_{\zeta|z} \quad (56a)$$

$$R_{\text{pass}} = \gamma_{\text{T1}}\mu_{z|w} \quad (56b)$$

so that $R = R_{\text{act}} + e^{-i2\phi_{\zeta|z}}R_{\text{pass}}$. Passive T1s are driven by anisotropic elastic strain $\mu_{z|w}$ (and hence stress anisotropy σ_{ww}). By contrast, active T1s can occur in the absence of macroscopic stress. Instead, they are driven by the tension anisotropy $\mu_{\zeta|z}$.

Thus, Eq. (54) qualitatively reproduces the mechanisms driving T1s on the cell level [18, 38]. There, the combined tension (active) and strain (passive) anisotropy determines when a cell-cell interface reaches zero length $\ell_{ij} = 0$, triggering a T1. The critical *microscopic* Beltrami coefficient for which $\ell_{ij} = 0$ can be worked out geometrically as $|\mu_{\zeta|w}^{\Delta}| = 1/2$ [18]. Here, the superscript Δ marks quantities on the single-triangle level. The Beltrami coefficients $\mu_{\zeta|z}$ and $\mu_{z|w}$ entering the continuum theory represent a macroscopic average over many tension triangles. The microscopic T1 threshold $|\mu_{\zeta|w}^{\Delta}| = 1/2$ implies the existence of a yield strain for passive T1s: below a critical $|\mu_{z|w}|$, the T1 rate γ_{T1} vanishes. More generally, γ_{T1} depends on the microscopic distribution of cell-level configurations $\mu_{\zeta|w}^{\Delta}$, which must be summarized by a suitable set of local order parameters. A mean-field approach [39] allows systematic calculation of γ_{T1} in terms of these order parameters, together with equations governing their dynamics.

4. T1s relax tension- and stress anisotropy

To complete the model for plasticity in the continuum, we need to address how cell rearrangements impact the tension metric \mathbf{g} . *A priori*, the flip flow due to cell rearrangements is a reparametrization—the tension manifold remains invariant (the macroscopic stress, depending only on \mathbf{g} and the physical BCs, also remains invariant). Edge flips in the triangulation pass between different triangulations that belong to the same stress state. However, T1s are not only an abstract “remeshing” of the tension manifold; they create a new cell interface whose tension dynamics are governed by specific (bio-)physical processes at the microscopic level. More precisely, by Eq. (53), edge flips change the tension anisotropy $\mu_{\zeta|z}$ (this is geometrically evident in the discrete setting; Fig. 8). The T1-induced change of tension anisotropy can then elicit subsequent dynamics of \mathbf{g} through the processes that govern the microscopic tensions.

For simplicity, in this section we linearize, assuming small strain and tension anisotropy, $|\zeta - z|, |z - w| \ll 1$, and further $\lambda_g \approx 1$. We can thus neglect the distinctions between the different coordinate systems ζ, z, w , and express everything z -coordinates. As a minimal model, we propose that passive T1-transitions remodel the tension metric, in addition to the active “drive” provided by \mathbf{m} .

$$\partial_t \log \mathbf{g} = \mathbf{m} + \mathbf{R}_{\text{pass}} \quad (57)$$

Hence, for the Beltrami coefficient, $\partial_t\mu_g = m_{zz}/4 + R_{\text{pass}}$.

As we now show, Eq. (57) captures the physically expected behavior for both active and passive plastic flow.

Using the passive T1-rate Eq. (56b), and relating deviatoric strain $\mu_{z|w}$ to the stress via Eq. (20):

$$\partial_t \mu_g = \frac{m_{zz}}{4} + \gamma_{T1} \mu_{z|w} = \frac{m_{zz}}{4} + \gamma_{T1} \frac{\sigma_{zz}}{2p_0 \lambda_g} \quad (58)$$

By a slight abuse of notation, we write σ_{zz} for the elastic stress in z -coordinates, which, of course, depends on the deformation w . On the other hand, changing the tension metric at fixed physical configurations changes the stress. We evaluate the Cauchy stress Eq. (4) in the current configuration, but using the time-incremented tension metric $\mathbf{g}(t + dt)$:

$$\boldsymbol{\sigma} = p_0 \boldsymbol{\epsilon}^T \cdot \sqrt{\mathbf{g}(z)} \cdot \boldsymbol{\epsilon} = p_0 \boldsymbol{\epsilon}^T \cdot \sqrt{\mathbb{I} + (\partial_t \mathbf{g}) dt} \cdot \boldsymbol{\epsilon} \quad (59)$$

(Strictly speaking, one should expand around $\mathbf{g}(w)$ and not $\mathbf{g}(z)$; we neglect the difference.) To linear order:

$$\partial_t \sigma_{zz} \Big|_{w=\text{const.}} = -\frac{p_0 \lambda_g}{2} (\partial_t \mu_g) \quad (60)$$

The minus sign comes from the $\pi/2$ rotation $\boldsymbol{\epsilon}$. Together, Eqs. (58), (60) result in effective Maxwell relaxation, with a source provided by \mathbf{m} :

$$\partial_t \sigma_{zz} \Big|_{w=\text{const.}} = -\gamma_{T1} \sigma_{ww} - 2p_0 m_{zz} \quad (61)$$

Eq. (61) describes how passive T1s relax stress when the cell positions w are pinned. Note that on the microscopic level, this corresponds to pinning cell centroids \mathbf{r}_i ; cell vertices \mathbf{r}_{ijk} are still free to move to establish local force balance. While T1s relax only the anisotropic stress, due to mechanical balance Eq. (22a), vanishing anisotropic stress also implies uniform isotropic stress gradients.

For the reference-state velocity field, the combination of stress relaxation and active driving manifests as an effective Stokes flow [cf. Eq. (43)]:

$$\begin{aligned} \Delta \dot{z}_\beta &= \frac{2\gamma_{T1}}{p_0} \partial_\alpha (\sigma_{\alpha\beta} - \frac{1}{2} \sigma_{\gamma\gamma} \delta_{\alpha\beta}) \\ &+ \partial_\alpha (m_{\alpha\beta} - \frac{1}{2} m_{\gamma\gamma} \delta_{\alpha\beta}) \end{aligned} \quad (62)$$

The anisotropic macroscopic stress enters with an effective viscosity $p_0/(2\gamma_{T1})$. Note that in many cases, γ_{T1} may vanish below a critical yield strain [38]. Eq. (62) thus combines active flow due to tension dynamics \mathbf{m} with viscous relaxation of elastic stress due to passive T1s. In the limiting cases discussed so far (free boundaries with flat tension metric; pinned cells) are particularly simple since one does not need to solve the effective elastic problem Eq. (44) for the physical flow \dot{w}_β (Sect. C3). In general, one must solve this non-local problem, as formally stated in Eq. (39), find the physical configuration w and thus the T1 rate $R = \gamma_{T1} \mu_{\zeta|w}$.

We now explore the physical consequences of the proposed model in the purely active and passive cases. Consider a conventional fluid foam, where $\mathbf{m} = 0$, as the paradigmatic case for passive T1s. External forces can build up deviatoric strain and thus macroscopic stress $\boldsymbol{\sigma}$,

while microscopic tensions remain constant. Eventually, strain causes T1s that relax macroscopic stress. Eq. (62) reproduces this physical intuition. Further, since all tensions equal the fluid's surface tension, $\mathbf{g} = \mathbf{a}$: T1s should directly modify the tension metric. This is precisely ensured by the dynamics Eq. (57).

Let us next consider the purely active case, $w = z$, i.e. $\mu_{z|w} = 0$. Here, T1s happen when $|\mu_{\zeta|z}|$ increases due to driving by m_{zz} (for example, positive mechanical feedback [19, 38] or a morphogen gradient [39, 40]). Substituting Eq. (57) into Eq. (53) shows that T1s relax tension anisotropy:

$$\frac{d}{dt} \mu_{\zeta|z} = \frac{1}{4} m_{zz} - R_{\text{act}} \quad (63)$$

Active T1s thus limit the tension anisotropy a tissue can attain. Steady active plastic flow results when driving and relaxation balance at a finite T1 rate. Active flow can take place at vanishing macroscopic stress and is therefore fundamentally different from conventional Maxwell viscoelasticity. Instead, it is characterized by sustained microscopic tension anisotropy, experimentally detectable as anisotropic junctional myosin [15].

To summarize, the present framework describes a tissue by two independently controlled metrics \mathbf{a} , \mathbf{g} . A kinematical prescription determines what happens during topological change (dynamics of $\mathbf{a}(t)$, keeping $\mathbf{g}(t)$ fixed). The dynamics of the tension metric \mathbf{g} depend on the specific model or biological context of interest. We showed that minimal and microscopically motivated choice, Eq. (57), naturally gives rise to Maxwell-like stress relaxation through passive T1s while active T1s relax tension anisotropy.

DISCUSSION

We have presented a continuum theory for active tension nets, a paradigmatic example of an *active solid*, where the local stress, rather than the local target shape, is the physical (or biological) control parameter. Microscopic tensions are purely active because passive stresses rapidly dissipate through molecular turnover. This distinguishes the type of active solid studied here from previous work where active stresses are added on top of a conventional (passive) elastic background [41–43] (see below).

From cell-level tensions to macroscopic stress. We have shown that the microscopic configuration of active tensions τ_{ij} defines, in the continuum limit, a Riemannian tension metric \mathbf{g} . This metric, together with the mechanical BCs, determines the macroscopic stress tensor $\boldsymbol{\sigma}$, and the positions w adopted by cells in mechanical equilibrium. By identifying the tension metric \mathbf{g} as the relevant macroscopic degree of freedom of active tension nets, our theory explains how local contractile activity translates into large-scale shape.

Crucially, many microscopic tension triangulations specify the *same* tension metric. They correspond to reparametrizations of the tension manifold and do not affect physical stress. Put differently, the macroscopic (i.e., tissue-scale) mechanical state only depends on the shape of the tension manifold, not how it is discretized by “painting” individual tension triangles onto it, like in a finite-element discretization of a partial differential equation. In particular, different triangulations of a region in the plane all define the same tension metric – only the shape of the region’s boundary is relevant. For a flat tension metric, the tissue configuration is fully encoded in the boundary shape and the traction forces. This “holographic” nature of emergent elasticity is also relevant in granular matter, where boundary forces constrain the ensemble of self-stresses in the bulk [44].

The microscopic cell shapes depend on the tension triangulation. Moreover, tensions are ultimately sensed and controlled at the cellular level. Therefore, their dynamics depend on the microscopic tension configuration. A continuum model, therefore, requires information in addition to \mathbf{g} . The most important piece is the adjacency metric \mathbf{a} , whose continuum dynamics captures cell rearrangements. While the tension metric \mathbf{g} determines the macroscopic mechanics, the local tension anisotropy is encoded in the “difference” of \mathbf{g} and \mathbf{a} – the shape of tension triangles. Overall, the present theory comprises the minimal description of tension nets in the continuum: The tension metric $\mathbf{g}(\xi)$ (equivalently, isothermal embedding $z(\xi, \bar{\xi})$ and curvature K_g) and the adjacent metric $\mathbf{a}(\xi)$, for a total of six degrees of freedom. The systematic description of stress and network topology in terms of Riemannian geometry and QC maps may prove useful to study other 2d materials with dynamic microscopic structure, such as granular matter.

Active plasticity. To describe tissue flow driven by adiabatic dynamics of active stress, one tracks the reference state $z(\xi, \bar{\xi}, t)$ of the evolving tension metric $\mathbf{g}(t)$. The resulting QC *adiabatic flow* \dot{z} is governed Eq. (42). Large deformations entail topological cell rearrangement. This raises the challenge of incorporating discrete topology into a continuum theory. On a cell level, topological information can be “geometrized” via the so-called “circle packing” of the cell adjacency graph, whose existence and uniqueness is guaranteed by the Koebe–Andreiev–Thurston theorem [45]. As explained in the companion paper [18], the circle packing is a “discrete” conformal embedding of the equilateral triangulation formed by the adjacency graph. In the continuum, it becomes the isothermal embedding $\zeta(\xi, \bar{\xi})$ of the adjacency metric \mathbf{a} , and cell rearrangement becomes the *flip flow* $\dot{\zeta}$. Tension dynamics, plasticity, and elastic deformation can thus be formulated as two coupled QC flows, Eqs. (42), and (52). This principled approach naturally incorporates the local tension configuration via the Jacobian $\partial_\zeta \mathbf{z}$.

Role and nature of active stress. Many continuum models for active and tissue mechanics posit a phenomenological active stress tensor σ^{act} [15–17], assumed

to be proportional to the local motor molecule concentration. Flow is driven by the divergence of σ^{act} , balanced against the passive stress σ^{pass} of a visco-elastic “background”. The balance of motor-generated force and viscosity sets the flow speed, and the tissue is instantaneously fluid (zero shear modulus).

By contrast, in the present model, there is no passive shear stress (all viscous and passive contributions are assumed to relax rapidly). Local motor molecule concentration is encoded in the tension metric \mathbf{g} . The resulting tensile stress σ depends both on \mathbf{g} and the embedding $\mathbf{r}(\xi)$ of active force dipoles into physical space via the stress-metric relation. It is therefore not consistent to prescribe an active stress *a priori*, independent of the cell configuration. The companion paper confirms this result by explicitly calculating the coarse graining the stress via the Batchelor formula (App. A gives a “preview”).

Plastic flow is caused by tension metric dynamics, and its speed is set by the *rate of change* of motor molecule concentration. The flow is adiabatic: the stress remains balanced throughout, and the system remodels from one solid configuration to the next. The tissue thus flows while remaining solid [46]. Notably, adiabatic flow takes the form of an effective Stokes equation, as in previous models describing tissue flow as viscous Stokes flow.

These distinctions have experimentally verifiable consequences. First, the present model predicts that the macroscopic stress remains isotropic during tissue flow (in the absence of external forces). A steady-state tension anisotropy, distinct from stress anisotropy, can emerge from the balance of anisotropy-increasing processes (such as mechanical feedback or morphogens) and resetting by T1s. This could be tested by laser ablations on supracellular scales. Second, it suggests that the speed of tissue flow is set not by the absolute levels of motor molecules and active tensions, but by their rate of change. These predictions rely on the separation of timescales between morphogenetic flow and relaxation of passive stress and mechanical equilibration. It will be important to explore what happens if this assumption is relaxed.

Emergent metric elasticity. On a formal level, the present theory has parallels with metric elasticity, where a Riemannian reference metric represents the rest lengths between adjacent material points [47–49], and deviations from these rest lengths in the physical configuration determine the elastic stress via a constitutive law. By contrast, the tension metric specifies the active stress (tension flux) between adjacent points. A stress-free reference state and an effective stress-strain relationship then *emerge* from the intrinsic stress configuration. The *stress-metric relation* determines the physical stress tensor in terms of the embedding of the tension metric given by the cell positions, i.e., the arrangement of active force dipoles in physical space. The present theory, therefore, furnishes the continuum limit of cell-level models dominated by *active* mechanics. By contrast, conventional metric elasticity is well-suited to describe the continuum limit of passive models (generalized spring-networks).

For instance, in the context of the well-known “area-perimeter” vertex model [7], Ref. [50] defined a network tensor that plays the role of the elastic reference metric. Plasticity can be modeled by relaxational dynamics of the reference metric [48].

Tissues on curved, topologically non-trivial, and dynamic surfaces. For simplicity, the present manuscript considers a tissue patch with a disk topology, embedded in the plane. If the tissue topology is non-trivial, new geometric modes and invariants appear. For example, on an annulus, there is a curl-free vector field that cannot be written as a potential gradient [51], and the annulus’ “aspect ratio” is conformally invariant [25]. Due to the important role of curl-free and conformal modes in our theory, this may have interesting physical consequences to be explored in future work. The geometric nature of the theory implies that it generalizes easily to tissues on curved surfaces, such as the ellipsoidal blastoderm of the *Drosophila*. To this end, the Euclidean metric $\delta_{\alpha\beta}$ in Eq. (11) must be replaced by the metric of the curved physical space. This is most conveniently done by parameterizing physical space with (yet another set of) isothermal coordinates. The reference configuration $z(\xi, \bar{\xi})$ is found as a conformal map between two curved surfaces – the tension- and physical manifold – and the mechanics is controlled by their *relative* geometry – e.g., the difference of Gaussian curvatures in Eq. (12).

In the above setting, the cells are still constrained to lie on a fixed (albeit curved) physical surface. More generally, one can consider tissues that form dynamic surfaces, embedded in three-dimensional space. One must additionally account for normal force balance, which couples in-plane stress and extrinsic physical curvature to normal pressure gradients [3]. This generalization is required in situations where in-plane contractility drives three-dimensional shape change of tissue sheets, e.g., during visceral organ morphogenesis [52].

Pressure effects and mechanical feedback. Gaussian curvature of the tension metric leads to pressure differentials, similar to residual stresses in metric elasticity due to an incompatible target metric. Interestingly, many tissues can avoid large pressure differentials and the potential instabilities they entail, like cell extrusion or rupture. On the cell level, pressures can be locally controlled via (negative) feedback loops [53] coupling tensions and intracellular pressure. A minimal mathematical model for such feedback is $\partial_t \mathbf{g} = -\beta(\Delta \log p/p_0)\mathbf{g} = -\beta K_g \mathbf{g}$, where β is a feedback coefficient and we used Eq. (12). Cells can hence implement a “flattening” Ricci flow [54] by modulating their overall contractile activity in response to intracellular pressure. In contrast to, e.g., Frank elasticity in liquid crystals, Ricci flow only acts on the “curvature part” of \mathbf{g} – the tension manifold can freely remodel in-plane to drive morphogenetic flows.

On the tissue level, pressure can be controlled via feedback through cell proliferation and growth [1, 55, 56], which in our formulation would act on the target cell density $n(\boldsymbol{\xi})$; Eq. (17). Analyzing such “adaptive” feedback

loops, and the combination of robustness and plasticity they confer, is an interesting direction for future research.

More generally, our findings have implications for how cells can sense and react to mechanical cues. We showed that the macroscopic stress σ is independent of the local tension configuration, and, therefore, “invisible” on a cell level. Instead, the cell-level “observables” are the tension anisotropy $\mu_{\zeta|z}$ and the intracellular pressure p . Cell shape anisotropy could be sensed by intracellular structures such as the nucleus, intermediate filaments, or microtubules.

Link to the microscopic ATN model. The link between the continuum theory and cell level (the discrete ATN model) is discussed in detail in a companion paper [18]. There, we exploit a theory of discrete conformal maps [57, 58] to bridge the gap between the continuum theory of the present manuscript and the mechanics at the cellular level. This theory constructs a discrete equivalent of the isothermal embedding $z(\xi, \bar{\xi})$. The isogonal (curl-free) and conformal modes identified by the continuum analysis reappear as the geometric soft modes which respect the microscopic force balance constraints [10, 59, 60], while the Liouville equation for the tension curvature leads to a generalized von Neumann law for the cell pressures. Coarse-graining the microscopic stress confirms the stress-metric relation Eq. (21). Thus, the “top-down” analysis presented here is independently confirmed by “bottom-up” coarse-graining.

Similarly, (active) plasticity, mediated by cell rearrangements, is captured by remodeling of the cell-adjacency graph. In the continuum, this graph is coarse-grained to the adjacency metric \mathbf{a} . The circle packing provides a discrete equivalent to the \mathbf{a} -isothermal coordinates (see paragraph on “active plastic flow” above). In the discrete setting, the condition for T1 transitions can be calculated explicitly from purely geometric considerations (a generalized “Delaunay criterion”), justifying the phenomenological T1 rate $\propto \mu_{\zeta|w}$ in amorphous tissue with negligible micro-structural order; Eq. (54). Micro-structural order can strongly influence T1 transitions, in which case additional order parameters become relevant [19]. A continuum theory for these order parameters and their relation to topological defects in the microscopic topology is an interesting direction for future research.

Outlook. While we have introduced our theory in the context of epithelial tissue mechanics, we believe it applies more broadly. Non-epithelial tissues, like those composed of protrusive, mesenchymal cells, do not form tension nets in the strict ATN sense, but their architecture and shape are also controlled by balancing active contractile stresses against bulk elasticity. Beyond the biological setting, 2d fluid or ferro-fluid foams [12, 61] correspond to the limiting case where all $\tau_{ij} = \tau = \text{const}$. Tension dynamics could be introduced, for instance, through chemical reactions within foam bubbles. As explained in the companion paper [18], there is also a close connection to granular materials and truss networks, which can be understood as the mechanical Legendre dual of

tension nets. In granular materials, one typically studies the ensemble of compatible (force-balanced) stress configurations for a given physical arrangement of particles. This is, in a sense, the dual of the problem considered in the present study. In future work, this Legendre duality might provide a starting point for continuum theories for granular matter. Indeed, previous phenomenological approaches postulate that granular materials can also be described by “emergent elasticity” [62]. Lastly, one may ask if the tension-metric-based approach can be generalized from tissue sheets to three-dimensional “volumetric” tissues. In 3d, Riemannian geometry becomes considerably richer [24].

To conclude, we believe that our theory provides a general framework for the emergent elasticity and plasticity of active solids, matter whose microscopic mechanics is

not governed by conventional constitutive laws but by independently controlled active forces. It quantitatively explains how these local active forces generate large-scale shape.

ACKNOWLEDGMENTS

We thank D. Cislo, A. Košmrlj, and H. Weyer for valuable feedback on the manuscript. B.I.S. acknowledges support of the NSF Physics (PoLS) grant #2210612. N.H.C. is supported by a PCTS fellowship. F.B. acknowledges funding from the Max Planck Society and the Gordon and Betty Moore Foundation post-doctoral fellowship (grant #2919).

-
- [1] S. F. Gilbert and M. J. F. Barresi, *Developmental Biology* (Sinauer Associates, Sunderland, Massachusetts, 2016).
- [2] C. Guillot and T. Lecuit, Mechanics of Epithelial Tissue Homeostasis and Morphogenesis, *Science* **340**, 1185 (2013).
- [3] L. D. Landau and E. M. Lifshitz, *Theory of Elasticity*, Course of Theoretical Physics, Vol. 7 (Pergamon Press, 1986).
- [4] G. F. Oster, J. D. Murray, and A. K. Harris, Mechanical aspects of mesenchymal morphogenesis, *Development* **78**, 83 (1983).
- [5] S. Alt, P. Ganguly, and G. Salbreux, Vertex models: From cell mechanics to tissue morphogenesis, *Philosophical Transactions of the Royal Society B: Biological Sciences* **372**, 20150520 (2017).
- [6] E. Coen and D. J. Cosgrove, The mechanics of plant morphogenesis, *Science* **379**, eade8055 (2023).
- [7] R. Farhadifar, J.-C. Röper, B. Aigouy, S. Eaton, and F. Jülicher, The Influence of Cell Mechanics, Cell-Cell Interactions, and Proliferation on Epithelial Packing, *Current Biology* **17**, 2095 (2007).
- [8] P. Agarwal and R. Zaidel-Bar, Principles of Actomyosin Regulation In Vivo, *Trends in Cell Biology* **29**, 150 (2019).
- [9] K. Bambardekar, R. Clément, O. Blanc, C. Chardès, and P.-F. Lenne, Direct laser manipulation reveals the mechanics of cell contacts in vivo, *Proceedings of the National Academy of Sciences* **112**, 1416 (2015).
- [10] N. Noll, M. Mani, I. Heemskerk, S. J. Streichan, and B. I. Shraiman, Active tension network model suggests an exotic mechanical state realized in epithelial tissues, *Nature Physics* **13**, 1221 (2017).
- [11] S. Kim, M. Pochitaloff, G. A. Stooke-Vaughan, and O. Campàs, Embryonic tissues as active foams, *Nature Physics* **17**, 859 (2021).
- [12] D. L. Weaire, D. L. Weaire, and S. Hutzler, *The Physics of Foams*, reprinted ed. (Clarendon Press, Oxford, 2005).
- [13] W. F. Baker and A. McRobie, eds., *The Geometry of Equilibrium: James Clerk Maxwell and 21st-Century Structural Mechanics*, 1st ed. (Cambridge University Press, 2025).
- [14] L. Cremona, *Le Figure Reciproche Nella Statica Grafica* (U. Hoepli, 1879).
- [15] S. J. Streichan, M. F. Lefebvre, N. Noll, E. F. Wieschaus, and B. I. Shraiman, Global morphogenetic flow is accurately predicted by the spatial distribution of myosin motors, *eLife* **7**, e27454 (2018).
- [16] M. Saadaoui, D. Rocancourt, J. Roussel, F. Corson, and J. Gros, A tensile ring drives tissue flows to shape the gastrulating amniote embryo, *Science* **367**, 453 (2020).
- [17] M. Serra, G. Serrano Nájera, M. Chuai, A. M. Plum, S. Santhosh, V. Spandan, C. J. Weijer, and L. Mahadevan, A mechanochemical model recapitulates distinct vertebrate gastrulation modes, *Science Advances* **9**, eadh8152 (2023).
- [18] N. Claussen, F. Brauns, and B. Shraiman, Coarse-graining active tension nets with discrete conformal geometry, arXiv 10.48550/arXiv.2601.14467 (2026).
- [19] N. H. Claussen, F. Brauns, and B. I. Shraiman, A geometric-tension-dynamics model of epithelial convergent extension, *Proceedings of the National Academy of Sciences* **121**, e2321928121 (2024).
- [20] J. McGrath, Y. Tardy, C. Dewey, J. Meister, and J. Hartwig, Simultaneous Measurements of Actin Filament Turnover, Filament Fraction, and Monomer Diffusion in Endothelial Cells, *Biophysical Journal* **75**, 2070 (1998).
- [21] The definition of the manifold structure and the continuum limit are explained in detail in our companion paper [18]. If tensions at a vertex violate the triangle inequality, this construction is not possible; however, as we will see below, such configurations are rapidly resolved by topological cell rearrangement.
- [22] Importantly, Eq. (4), and its consequence Eq. (20), are *not* “transformation laws” that relate the stress tensor in different coordinates (akin to Cauchy and Piola-Kirchhoff stress [63]). Rather, they describe how the Cauchy stress depends on deformation, like a stress-strain relation in conventional elasticity.
- [23] D. J. Cislo, A. Pavlopoulos, and B. I. Shraiman, “Morphogenetic Action” Principle for 3D Shape Formation by the Growth of Thin Sheets, *Physical Review X* **15**, 021068 (2025).
- [24] J. M. Lee, *Introduction to Riemannian Manifolds*, Grad-

- uate Texts in Mathematics, Vol. 176 (Springer International Publishing, Cham, 2018).
- [25] L. Ahlfors, *Lectures on Quasiconformal Mappings* (D. van Nostrand Company, Princeton, NJ, 1966).
- [26] N. I. Muskhelishvili, *Some Basic Problems of the Mathematical Theory of Elasticity* (Springer Netherlands, Dordrecht, 1977).
- [27] The “incompatibility” of the tension manifold with the cell density that gives rise to residual stresses is distinct from the geometric incompatibility of a curved “reference metric” with a flat physical configuration found in the metric elasticity framework [47]. In the latter, the reference metric encodes local rest lengths in the material.
- [28] F. De Goes, P. Memari, P. Mullen, and M. Desbrun, Weighted Triangulations for Geometry Processing, *ACM Transactions on Graphics* **33**, 1 (2014).
- [29] J. Stickforth, A simplified derivation of Kolosov’s theorem of the complex formulation of plane elasticity, *Journal of Elasticity* **5**, 79 (1975).
- [30] More precisely, it is the potential of the inverse mapping $z(w, \bar{w}) = w + 2\partial_w \theta$ which defines the Airy function. To linear order, this only changes a sign.
- [31] Indeed, the biharmonic Eq. (35) can be written variationally: any solution must minimize the functional $\int [(\Delta\theta)^2 + \theta \Delta(B^{-1} \log \lambda_g + \delta n)] d^2 w$. Using $\text{Tr} \boldsymbol{\sigma}^{\text{tot}} = \Delta\theta$ and integrating by parts, the stress thus minimizes $\int [(\text{Tr} \boldsymbol{\sigma})^2 + (\text{Tr} \boldsymbol{\sigma})(B^{-1} \log \lambda_g + \delta n)] d^2 w$.
- [32] K. Irvine and E. Wieschaus, Cell intercalation during *Drosophila* germband extension and its regulation by pair-rule segmentation genes, *Development* **120**, 827 (1994).
- [33] C.-P. Heisenberg and Y. Bellaïche, Forces in Tissue Morphogenesis and Patterning, *Cell* **153**, 948 (2013).
- [34] M. F. Lefebvre, N. H. Claussen, N. P. Mitchell, H. J. Gustafson, and S. J. Streichan, Geometric control of myosin II orientation during axis elongation, *eLife* **12**, e78787 (2023).
- [35] P. Caldarelli, A. Chamolly, A. Villedieu, O. Alegria-Prévo, C. Phan, J. Gros, and F. Corson, Self-organized tissue mechanics underlie embryonic regulation, *Nature* **633**, 887 (2024).
- [36] In an equilateral triangulation, a coordination number $\neq 6$ implies a nonzero angle deficit around a vertex, and hence non-zero Gaussian curvature concentrated at such vertices.
- [37] Microscopically, the cell area in an equilateral triangulation is proportional to the coordination number. Hence, strictly speaking, $\mathbf{a} \mapsto \mathbf{a}/n_0$ only holds if there is no large-scale coordination number gradient.
- [38] F. Brauns, N. H. Claussen, E. F. Wieschaus, and B. I. Shraiman, The Geometric Basis of Epithelial Convergent Extension, *eLife* [10.7554/eLife.95521.1](https://doi.org/10.7554/eLife.95521.1) (2024).
- [39] N. H. Claussen and F. Brauns, Mean-Field Model for Active Plastic Flow of Epithelial Tissue, *PRX Life* **3**, 023002 (2025).
- [40] M. Ibrahimi and M. Merkel, Deforming polar active matter in a scalar field gradient, *New Journal of Physics* **25**, 013022 (2023).
- [41] A. Maitra and S. Ramaswamy, Oriented Active Solids, *Physical Review Letters* **123**, 238001 (2019).
- [42] P. Baconnier, D. Shohat, C. H. López, C. Coulais, V. Démary, G. Düring, and O. Dauchot, Selective and collective actuation in active solids, *Nature Physics* **18**, 1234 (2022).
- [43] F. Brauns, M. O’Leary, A. Hernandez, M. J. Bowick, and M. C. Marchetti, Active Solids: Topological Defect Self-Propulsion Without Flow, *Physical Review Letters* **136**, 058302 (2026).
- [44] E. DeGiuli, Edwards field theory for glasses and granular matter, *Physical Review E* **98**, 033001 (2018).
- [45] K. Stephenson, *Introduction to Circle Packing: The Theory of Discrete Analytic Functions* (Cambridge University Press, Cambridge, 2005).
- [46] Note, however, that the yield strain becomes highly anisotropic during active plastic flow. Due to the ongoing T1 transitions, there is a large number of cells near the T1 threshold, and the yield strain parallel to tension anisotropy can become very small.
- [47] E. Efrati, E. Sharon, and R. Kupferman, Elastic theory of unconstrained non-Euclidean plates, *Journal of the Mechanics and Physics of Solids* **57**, 762 (2009).
- [48] E. Efrati, E. Sharon, and R. Kupferman, The metric description of elasticity in residually stressed soft materials, *Soft Matter* **9**, 8187 (2013).
- [49] R. Kupferman, M. Moshe, and J. P. Solomon, Metric Description of Singular Defects in Isotropic Materials, *Archive for Rational Mechanics and Analysis* **216**, 1009 (2015).
- [50] D. Grossman and J.-F. Joanny, Instabilities and Geometry of Growing Tissues, *Physical Review Letters* **129**, 048102 (2022).
- [51] J. M. Lee, *Introduction to Smooth Manifolds*, Graduate Texts in Mathematics, Vol. 218 (Springer New York, New York, NY, 2012).
- [52] N. P. Mitchell, D. J. Cislo, S. Shankar, Y. Lin, B. I. Shraiman, and S. J. Streichan, Visceral organ morphogenesis via calcium-patterned muscle constrictions, *eLife* **11**, e77355 (2022).
- [53] The pressure feedback discussed here operates quasi-statically and requires a non-zero bulk modulus to build up pressure gradients. By contrast, in a compressible tissue, tension incompatibility causes secular elongation or contraction of cell-cell interfaces, requiring a different stabilizing mechanism (see Ref. [10]).
- [54] T. Tao, Ricci flow, in *The Princeton Companion to Mathematics* (Princeton University Press, Princeton, NJ, 2008) pp. 279–281.
- [55] B. I. Shraiman, Mechanical feedback as a possible regulator of tissue growth, *Proceedings of the National Academy of Sciences* **102**, 3318 (2005).
- [56] K. D. Irvine and B. I. Shraiman, Mechanical control of growth: Ideas, facts and challenges, *Development* **144**, 4238 (2017).
- [57] B. Springborn, P. Schröder, and U. Pinkall, Conformal equivalence of triangle meshes, *ACM Transactions on Graphics* **27**, 1 (2008).
- [58] A. I. Bobenko and C. O. R. Lutz, Decorated Discrete Conformal Maps and Convex Polyhedral Cusps, *International Mathematics Research Notices* **2024**, 9505 (2024).
- [59] C. Moukarzel, Geometrical consequences of foam equilibrium, *Physical Review E* **55**, 6866 (1997).
- [60] N. Noll, S. J. Streichan, and B. I. Shraiman, Variational Method for Image-Based Inference of Internal Stress in Epithelial Tissues, *Physical Review X* **10**, 011072 (2020).
- [61] F. Elias, J.-C. Bacri, F. H. De Mougins, and T. Spengler, Two-dimensional ferrofluid foam in an external force field: Gravity arches and topological defects, *Philosophical Magazine Letters* **79**, 389 (1999).

- [62] J. N. Nampoothiri, M. D’Eon, K. Ramola, B. Chakraborty, and S. Bhattacharjee, Tensor electromagnetism and emergent elasticity in jammed solids, *Physical Review E* **106**, 065004 (2022).
- [63] J. E. Marsden, T. J. R. Hughes, and D. E. Carlson, Mathematical Foundations of Elasticity, *Journal of Applied Mechanics* **51**, 946 (1984).
- [64] S. Alexander, Amorphous solids: Their structure, lattice dynamics and elasticity, *Physics Reports* **296**, 65 (1998).
- [65] G. K. Batchelor and J. T. Green, The determination of the bulk stress in a suspension of spherical particles to order c^2 , *Journal of Fluid Mechanics* **56**, 401 (1972).
- [66] L. Ahlfors, *Complex Analysis: An Introduction to the Theory of Analytic Functions of One Complex Variable, Third Edition*, 3rd ed. (McGraw-Hill, Inc., New York, 1979).
- [67] R. Sawhney and K. Crane, Boundary First Flattening, *ACM Transactions on Graphics* **37**, 1 (2018), arXiv:1704.06873 [cs].

Appendix A: Discrete-continuum correspondence for a “rectangular foam”

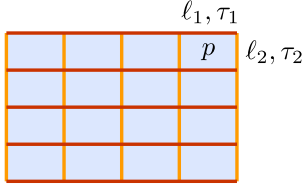


FIG. 5. “Rectangular foam” with anisotropic surface tensions τ_1 on horizontal edges and τ_2 on vertical edges.

Here, we discuss a minimal “cartoon” example that connects the continuum theory to the discrete active tension network model. It generalizes the “square foam” introduced in [64] and is composed of identical rectangular cells with internal pressure p and possibly anisotropic interfacial tensions τ_1, τ_2 on horizontal and vertical edges (see Fig. 5.) Batchelor’s formula [65] (treating each edge as a force dipole) gives the macroscopic tensile stress

$$\boldsymbol{\sigma} = \frac{1}{a} \sum_i \ell_i \tau_i \hat{\mathbf{e}}_i \otimes \hat{\mathbf{e}}_i = \frac{1}{\ell_1 \ell_2} \begin{pmatrix} \tau_1 \ell_1 & 0 \\ 0 & \tau_2 \ell_2 \end{pmatrix} \quad (\text{A1})$$

where ℓ_i are the edge lengths. In an unloaded state (no external forces), force balance implies $0 = dE = \tau_1 d\ell_1 + \tau_2 d\ell_2 - pd(\ell_1 \ell_2)$ and therefore $\ell_{1,2}^0 = \tau_{2,1}/p$. Hence $\sigma_{\alpha\beta} = p\delta_{\alpha\beta}$ and the total stress $\boldsymbol{\sigma}^{\text{tot}} = \sigma_{\alpha\beta} - p\delta_{\alpha\beta}$ vanishes identically, as expected in an unloaded uniform state. It is worth emphasizing that the configuration $\ell_{1,2}^0$ is an effective stress-free reference state: the tensions τ_1, τ_2 are length-independent. Deforming the system away from this reference state leads to a non-zero total stress

$$\boldsymbol{\sigma}^{\text{tot}} \approx -p \begin{pmatrix} \frac{\ell_2}{\ell_2^0} - 1 & 0 \\ 0 & \frac{\ell_1}{\ell_1^0} - 1 \end{pmatrix} \quad (\text{A2})$$

Recognizing the elements of the strain tensor, we read off the *effective* shear and bulk moduli $\mu_{\text{eff}} = p/2$ and $B_{\text{eff}} = -p/2$. Thus, the elastic response is evidently isotropic, despite the underlying microscopic anisotropy. Moreover, the negative bulk modulus indicates mechanical instability. This instability is a consequence of simultaneously prescribing edge tensions and pressure. It implies that pressure cannot be prescribed, but must derive from an equation of state $p = P(n)$, where $n = 1/(\ell_1 \ell_2)$ is the cell density. To find the unloaded state, one needs to solve self-consistently for $p_0 = P(n_0) = P(p_0^2/\tau_1 \tau_2)$. The linearization of the equation of state around n_0 then yields an additional contribution to the effective bulk modulus $B_{\text{eff}} = -\frac{p_0}{2} + P'(n_0)$, restoring stability for sufficiently large $P(n_0) > p_0/2$.

We conclude our discussion by illustrating the tension metric and its isothermal embedding. Consider Lagrangian coordinates $\boldsymbol{\xi}$ enumerating rows and columns of cells. In these coordinates, we can encode the edge tensions in the tension metric

$$\mathbf{g}(\boldsymbol{\xi}) = \begin{pmatrix} \tau_2^2 & 0 \\ 0 & \tau_1^2 \end{pmatrix}. \quad (\text{A3})$$

Note that τ_2 appears in the (1, 1) entry since the tension metric encodes tension on edges *perpendicular* to a displacement vector $d\boldsymbol{\xi}$. In the physical configuration, specified by ℓ_1, ℓ_2 , the metric reads

$$\mathbf{g}(\mathbf{r}) = \begin{pmatrix} \tau_2^2/\ell_1^2 & 0 \\ 0 & \tau_1^2/\ell_2^2 \end{pmatrix}. \quad (\text{A4})$$

This ensures that $\tau_i^2 = g_{\alpha\beta} dr_{i,\alpha} dr_{i,\beta}$, $i = 1, 2$, where dr_i is the physical vector connecting two adjacent cells. Crucially, comparing Eqs. (A1) and (A4) recovers the stress-metric relation Eq. (4):

$$\boldsymbol{\sigma}^2(\mathbf{r}) = \begin{pmatrix} \tau_1^2/\ell_2^2 & 0 \\ 0 & \tau_2^2/\ell_1^2 \end{pmatrix} = \boldsymbol{\epsilon}^T \cdot \mathbf{g}(\mathbf{r}) \cdot \boldsymbol{\epsilon} \quad (\text{A5})$$

To find the isothermal embedding where $\mathbf{g} \propto \mathbb{I}$, one thus scales the spatial directions by the respective tensions: $p_0 \mathbf{r}_1 = \tau_2 \boldsymbol{\xi}_1$, $p_0 \mathbf{r}_2 = \tau_1 \boldsymbol{\xi}_2$. This recovers the stress-free reference calculated above.

This toy example already captures key elements of actual tension networks and foams, which are locally hexagonal instead of rectangular, and whose tension configuration is not spatially uniform. The calculation of the effective stress of these more complex networks is a key part of the companion paper [18].

Appendix B: Examples for the static problem

We provide two concrete examples to illustrate the continuum equations derived in the main text. Since the static problem is mathematically equivalent to linear elasticity, these examples serve to clarify the definitions of the tension- and adjacency metrics and the logic of the mapping from the tension manifold to the physical state.

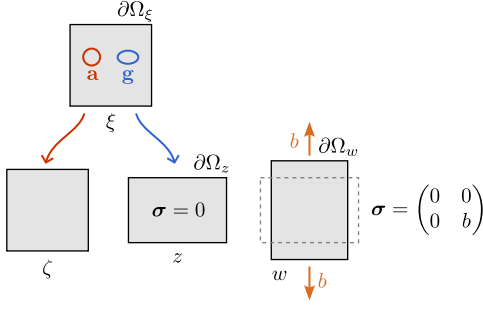


FIG. 6. Elementary example for tension- and adjacency metrics.

1. Statics: flat tension metric

As a first example, we revisit the rectangular foam from App. A now in the continuum, as illustrated in Fig. 6. Let the adjacency metric be the Euclidean metric, corresponding to uniformly distributed isotropic cells. The \mathbf{a} -isothermal ζ coordinates are therefore simply Cartesian coordinates in the unit square $0 \leq \zeta_1, \zeta_2 \leq 1$. In this square shape, the cell density is uniform, and cell shapes are isotropic. Next, we need to specify the active tension configuration, i.e., the tension metric g . In this example, we consider an anisotropic metric, $g_{\zeta\zeta} = 2$, $g_{\zeta\bar{\zeta}} = s$ where the real parameter $0 < s \ll 1$ determines the strength of anisotropy. In Cartesian notation, $\mathbf{g}(\zeta_1, \zeta_2) = \text{diag}[1+s, 1-s]$ corresponding to $\tau_1^2 = 1-s$, $\tau_2^2 = 1+s$ in the notation of App. A. Microscopically, this tension metric means that vertical cell-cell interfaces are under higher tension than horizontal ones, since the tension metric encodes the tension on interfaces transverse to a line element $d\mathbf{r}$ (cf. Fig. 2). The Beltrami coefficient reads $\mu_g = s/(2 + \sqrt{(1+s)(1-s)}) \approx s/4$, where the approximation is for $s \ll 1$. To remove this anisotropy, the \mathbf{g} -isothermal coordinates need to create a corresponding shear, $z(\zeta, \bar{\zeta}) = \zeta + \mu_g \bar{\zeta}$. This fulfills the Beltrami Eq. (10). In Cartesian notation, $\mathbf{z} = \text{diag}[1+\mu_g, 1-\mu_g] \cdot \zeta$.

Since $\det \mathbf{g} \approx 1$, tension and cell densities are (approximately) equal in this example. Further, since \mathbf{g} is constant, it has no curvature, $K_g = 0$: the z -configuration has constant cell density and constant pressure p_0 . It is therefore mechanically balanced in the absence of external forces. In other words, $u_\alpha = 0$ solves the linear elasticity force-balance equation Eq. (32). This example illustrates how tension anisotropy controls tissue shape.

Let us now consider applying a constant boundary traction force $b_1 = 0, b_2 = \pm b$ to the upper (+) and lower (-) edges of the rectangular tissue patch, (the left and right sides remain free). This results in a potential displacement $u_\alpha = f_\alpha + \partial_\alpha \theta$ from the tension reference z to the physical configuration $w = z + u(z, \bar{z})$. By Eq. (35), the potential θ must be biharmonic, $\Delta^2 \theta = 0$. The traction forces $\sigma \cdot \mathbf{n}_\pm = [0, \pm b]$ at the top and bottom edges require $\sigma_{22}|_\pm = p_0(\partial_1^2 \theta)|_\pm = b$. We can hence

take $\theta = b \text{Re}[z]^2/(2p_0)$, which implies a uniform stress $\sigma = \text{diag}(0, b)$ in the bulk and, thus, also fulfills the free BCs on the left and right edge. This result is expected by simple physical reasoning. To ensure that the displacement u_α is incompressible, we add a conformal contribution $f(z) = -bz$ (in this case, simply a uniform scaling).

2. Statics: non-flat tension metric

Next, we study an example where the tension metric has curvature. We consider a circular tissue patch. The adjacency metric is the Euclidean metric in the unit disk. The \mathbf{a} -isothermal ζ -coordinates are simply Cartesian coordinates. In ζ -coordinates, the cell density is uniform. We now define the tension metric by:

$$(g_{\alpha\beta}) = \begin{pmatrix} 1 + \zeta_1^2/h^2 & \zeta_1\zeta_2/h^2 \\ \zeta_1\zeta_2/h^2 & 1 + \zeta_2^2/h^2 \end{pmatrix}, \quad h(\zeta, \bar{\zeta})^2 = 1 - \zeta\bar{\zeta} \quad (\text{B1})$$

We use round brackets to highlight that this matrix uses Cartesian, not complexified, coordinates. It is the metric of a unit hemisphere, a height h above the unit circle in Monge parametrization (Fig. 7). Since $\det \mathbf{g} = 1/h(\zeta, \bar{\zeta})^2$, the ‘‘tension density’’ is higher at the margin than at the center.

We now need to find the transformation $z(\zeta, \bar{\zeta})$ that makes this tension metric isotropic. Because of rotation symmetry, we expect a radial dilation. The g -isothermal coordinates are given by the stereographic projection [66] of the hemisphere, which is a conformal map:

$$z(\zeta, \bar{\zeta}) = \frac{\zeta}{1 + h(\zeta, \bar{\zeta})} \quad (\text{B2})$$

The conformal factor reads $\lambda_g(z, \bar{z}) = 2/(1 + z\bar{z})$, which fulfills $\lambda_g = 1$ on the boundary. By Eq. (12), the curvature is constant, $K_g = 1$, as expected for a unit sphere.

Due to curvature, area distortion (and thus cell density gradients) in the tension reference state z are unavoidable. For an incompressible tissue, these must be compensated by an isogonal displacement $w - z = u = f(z) + 2\bar{\partial}_z \theta$; Eq. (32). Incompressibility means $(\det \mathbf{D}w)^{-1} \sqrt{\det g(z, \bar{z})} = 1$ where $(Dw)_{\alpha\beta} = \partial_\alpha w_\beta$ is the Jacobian. Expanding $\det \mathbf{D}w = \det[\delta_{\alpha\beta} + \partial_\alpha u_\beta]$ with $w_\alpha = f_\alpha + \partial_\alpha \theta$ to linear order:

$$\Delta \theta + \partial_\alpha f_\alpha = \frac{2}{z\bar{z} - 1} \quad (\text{B3})$$

We now obtain a rotation-symmetric solution to Eq. (B3) as a function of $r = \sqrt{z\bar{z}}$. First, the only rotation-symmetric conformal mode is a uniform scaling $f(z) = Cz$. Further, we fix an irrelevant global constant by setting $\theta(0) = 0$. The equation for $\theta(r)$ then reads

$$\Delta \theta(r) + C = \frac{2}{1 + r^2} \quad (\text{B4})$$

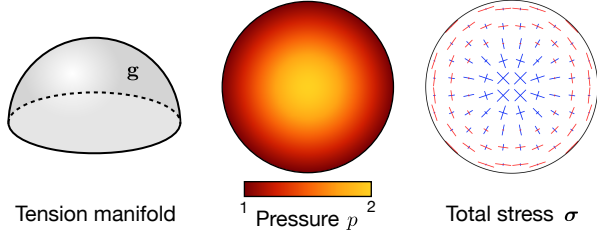


FIG. 7. A half-sphere tension manifold induces a non-constant pressure field and a non-vanishing total stress even for traction-free boundary conditions. Note that the total stress is isotropic in the center and purely tangential along the boundary, as is required by the traction-free boundary conditions.

with BCs $\theta(0) = 0$, $\partial_r\theta(r=0) = 0$, and $\partial_r\theta(r=R) = 0$. The last condition follows from $\sigma \cdot \mathbf{n} = 0$ (vanishing traction forces at the boundary). Via the strain $C = \partial_\alpha f_\alpha$ of the conformal map, we fulfill the last BC. Equation (B4) is solved by $\theta(r) = \frac{1}{4}[-r^2 + 2\log(1+r^2)]$ with $C = 1$.

Within the disk, $\sigma_{\alpha\beta}^{\text{tot}} = -p_0 \epsilon_{\alpha\gamma} \epsilon_{\beta\delta} \partial_\gamma \partial_\delta \theta \neq 0$; Eq. (34). These internal residual stresses, shown in Fig. 7, result from curvature of the tension manifold. Importantly, such stresses will also be present for finite cell compressibility. In the limit of fully compressible cells, no force-balanced configuration exists because sustaining the pressure field implied by the tension manifold curvature requires a finite cell compressibility.

Appendix C: Change of curvature radius by a conformal map

Here, we compute the change of a line's curvature radius R by a conformal map $z \mapsto f(z)$ [66]. Consider a line $z(t)$ with normal \mathbf{n} . The rotation of the local normal is given by the vorticity $\omega = \arg \partial_z f$. Moving a step dt along the transformed curve $f(z(t))$, the tangent $i\mathbf{n}$ rotates by an angle $d\phi = \omega(f(z(t+dt))) - \omega(f(z(t))) = (i\mathbf{n}) \cdot 2\bar{\partial}_z \omega dt$. Due to the scaling factor $|\partial_z f|$, the arc length is $|\partial_z f| dt$. Altogether, the curvature radius reads:

$$\frac{1}{R} = \frac{d\phi}{d(\lambda t)} = \frac{i\mathbf{n}}{|\partial_z f|} \cdot 2\bar{\partial}_z \arg \partial_z f = \mathbf{n} \cdot 2\bar{\partial}_z |\partial_z f| \quad (\text{C1})$$

Appendix D: The isogonal-conformal decomposition

Here, we show that any vector field u_α that fulfills the solvability condition $\Delta(\epsilon_{\alpha\beta} \partial_\beta u_\alpha) = 0$ (the vorticity is harmonic) can be decomposed as $u_\alpha = \partial_\alpha \theta + f_\alpha$, where f_α is a conformal vector field. In contrast to the familiar Helmholtz decomposition into curl- and divergence-free parts, this decomposition is only possible if the solvability condition is fulfilled. For example, a solenoidal vector field $u_\alpha = \epsilon_{\alpha\beta} \partial_\beta \psi$ must have $\Delta^2 \psi = 0$.

We first aim to identify $\theta^{(1)}$ so that $f_\alpha^{(1)} = u_\alpha - \partial_\alpha \theta^{(1)}$ is harmonic. We must solve $\Delta \partial_\alpha \theta^{(1)} = \Delta u_\alpha$. This is solvable if the curl $\epsilon_{\alpha\beta} \partial_\beta$ of the RHS vanishes, which is the condition we assumed. Next, we aim to make the two components f_1, f_2 not just harmonic, but conjugate harmonic to fulfill the Cauchy–Riemann equations. We shift again $f_\alpha^{(1)} \mapsto f_\alpha^{(2)} = f_\alpha^{(1)} - \partial_\alpha \theta^{(2)}$. The Cauchy–Riemann equations imply that the deviatoric strain of $f^{(2)}$ must vanish. Hence, $\theta^{(2)}$ must fulfill

$$\partial_\alpha \partial_\beta \theta^{(2)} = \frac{1}{2} \left(\partial_\alpha f_\beta^{(1)} + \partial_\beta f_\alpha^{(1)} - \partial_\gamma f_\gamma^{(1)} \delta_{\alpha\beta} \right) \quad (\text{D1})$$

Since the curl of the LHS is $\epsilon_{\beta\gamma} \partial_\gamma \partial_\alpha \partial_\beta \theta^{(2)} = 0$, the curl of the RHS must also vanish:

$$\begin{aligned} \epsilon_{\beta\gamma} \partial_\gamma \left(\partial_\alpha f_\beta^{(1)} + \partial_\beta f_\alpha^{(1)} - \partial_\delta f_\delta^{(1)} \delta_{\alpha\beta} \right) \\ = (\epsilon_{\alpha\gamma} \partial_\gamma \partial_\beta - \epsilon_{\beta\gamma} \partial_\gamma \partial_\alpha) f_\beta^{(1)} = \epsilon_{\alpha\beta} \partial_\gamma^2 f_\beta = 0 \end{aligned} \quad (\text{D2})$$

since $f_\beta^{(1)}$ is already harmonic. Hence, we arrive at the desired conformal-isogonal decomposition $u_\alpha = \partial_\alpha \theta + f_\alpha^{(2)} = \partial_\alpha(\theta^{(1)} + \theta^{(2)}) + (u_\alpha - \partial_\alpha \theta^{(1)} - \partial_\alpha \theta^{(2)})$.

Appendix E: Boundary conditions

Here, we show that the two modes compatible with force balance, the curl-free and conformal modes, are sufficient to accommodate arbitrary mechanical BCs. Indeed, the curl-free mode is already sufficient to accommodate arbitrary boundary displacements $\mathbf{u}_{\partial\Omega}$ (except for global rotations, which are conformal). Write $\mathbf{u}_{\partial\Omega}(s) = u_s \hat{\mathbf{s}} + u_n \hat{\mathbf{n}}$, where s is the arc length and $\hat{\mathbf{s}}, \hat{\mathbf{n}}$ are the tangent and normal. Since $\mathbf{u} = \nabla \theta$ the isogonal potential must fulfill

$$\partial_s \theta = u_s, \quad \partial_n \theta = u_n \quad (\text{E1})$$

along the boundary. We can therefore find θ along the boundary by integrating u_s

$$\theta|_{\partial\Omega}(s) = \int_0^s ds' u_s(s') \quad (\text{E2})$$

Via a global rotation, we can ensure the requirement that

$$\oint ds u_s = \oint ds \cdot \mathbf{u}^{(b)}(s) = 0 \quad (\text{E3})$$

To fulfill $\partial_n \theta = u_n$, we continue θ into the bulk with slope u_n :

$$\theta(\mathbf{b}(s) + dn \mathbf{n}) = \theta|_{\partial\Omega}(s) + dn u_n(s), \quad (\text{E4})$$

where $\mathbf{b}(s)$ parametrizes the boundary curve and dn is the (infinitesimal) distance from the boundary.

By contrast, conformal deformations alone are insufficient. A flat conformal map f is fully specified by its conformal factor $|\partial_z f|$, which obeys the Liouville equation

$\Delta \log |\partial_z f| = 0$. This Poisson problem admits prescribing either Dirichlet conditions $|\partial_z f|_{\partial\Omega}$, or Neumann conditions $\partial_{\mathbf{n}}|\partial_z f|_{\partial\Omega}$ (the boundary curvature), but not both simultaneously. Equivalently, one can specify BCs for one of the two components f_α – the second component is fixed by the Cauchy-Riemann equations $\partial_\alpha f_1 = \epsilon_{\alpha\beta} \partial_\beta f_2$.

For example, consider the unit disk in complex polar coordinates $z = re^{i\phi}$. Conformal maps f are analytic, $f(z) = \sum_{n \geq 0} \frac{f^{(n)}}{n!} z^n$. Importantly, the sum is restricted to $n \geq 0$: hence, the boundary value $f(e^{i\phi})$ has only non-negative Fourier coefficients. A boundary displacement with negative Fourier coefficients cannot be extended to a conformal deformation of the disk. For example, pure shear $\mathbf{u}|_{\partial\Omega} \propto e^{-i\phi} = x\hat{\mathbf{x}} - y\hat{\mathbf{y}}$ is incompatible with a conformal deformation.

Boundary conditions for the Beltrami equation. In the context of the Beltrami equation Eq. (10), the BCs fix the conformal contribution to $z(\xi, \bar{\xi})$. Therefore, the Beltrami equation also admits a single BC only, e.g., the natural BC for $|\partial_\xi z|$, Eq. (14). Indeed, the example Appendix B 1 makes it clear that it is impossible to make the tension metric isotropic while keeping the boundaries clamped. The Beltrami equation must be contrasted with the elasticity problem for the physical configuration w , which admits two boundary conditions.

Appendix F: Integrating the quasiconformal flow via Green's functions

The quasiconformal flow Eq. (42) describes the flow $\dot{z}(z, \bar{z})$ of the stress-free reference state z due to the dynamics of the tension metric. Note that for any solution $\dot{z}(z, \bar{z})$ of Eq. (42), $\dot{z}(z, \bar{z}) + f(z)$ for a conformal $f(z)$ is also a solution. The BCs fix this conformal component. In the main text, we used natural BCs, $\lambda_g|_{\partial\Omega} = 1$. This minimizes the deformation of the embedding $z(\zeta, \bar{\zeta})$ and the pressure gradients in the reference state, providing a convenient starting point for linearization; Eq. (31). The shape of the natural domain boundary $\partial\Omega$ is, however, time-dependent.

Instead, one can fix the conformal component by demanding that the isothermal coordinates map the tension manifold to the unit disk. We denote these “disk” isothermal coordinates by \hat{z} , with $D = \{|\hat{z}| \leq 1\}$. Then, Eq. (42) can be solved by a fixed Green's function [25]:

$$\dot{\hat{z}}(\hat{z}, \bar{\hat{z}}) = \frac{1}{2\pi i} \int \int_D d\hat{z}' d\bar{\hat{z}}' G(\hat{z}, \hat{z}') \partial_t \mu_g(\hat{z}', \bar{\hat{z}}'), \quad (\text{F1})$$

$$G(\hat{z}, \hat{z}') = \frac{\hat{z}(\hat{z} - 1)}{(\hat{z}' - \hat{z})\hat{z}'(\hat{z}' - 1)} \quad (\text{F2})$$

Eq. (F1) also allows the explicit computation of the topological flow due to local cell rearrangement. In summary, the dynamics of the reference state becomes a QC flow $\dot{\hat{z}}$ on the disk D , and is analytically tractable. The price to be paid is that the deformation from the reference to the physical state is now, in general, very large.

It is therefore useful to keep track of the conformal map from the disk D to the natural domain Ω , which we denote $\hat{z} \mapsto z(\hat{z})$. To do so, one can follow the approach of Ref. [67] and first determine the image of the disk boundary ∂D . Denoting the conformal factor by $\lambda_{\hat{z}|z} = |\partial_{\hat{z}} z|$, the natural BCs require $\lambda_{\hat{z}|z}^2|_{\partial D} = \lambda_g^2(\hat{z}, \bar{\hat{z}})|_{\partial D}$ on the disk boundary. We now note that $\Delta \log \lambda_{\hat{z}|z} = 0$, since $\log \lambda_{\hat{z}|z}$ is the real part of the analytic function $\log(\partial_{\hat{z}} z)$. Therefore, we can obtain $\log \lambda_{\hat{z}|z}$ on the entire disk by convolution with the Poisson kernel $P(\hat{z}, \hat{z}')$ as

$$\log \lambda_{\hat{z}|z}(\hat{z}) = (2\pi)^{-1} \int_{\partial D} d\hat{z}' P(\hat{z}, \hat{z}') \log \lambda_{\hat{z}|z}(\hat{z}'), \quad (\text{F3})$$

$$P(\hat{z}, \hat{z}') = \text{Re}[(\hat{z} + \hat{z}')/(\hat{z} - \hat{z}')] \quad (\text{F4})$$

In particular, the normal derivative on the boundary is $\partial_{\mathbf{n}} \log \lambda_{\hat{z}|z}|_{\partial D} = (2\pi)^{-1} \int_{\partial D} d\hat{z}' \log \lambda_{\hat{z}|z}(\hat{z}') \text{Re} \left[\frac{\hat{z}\hat{z}'}{(\hat{z} - \hat{z}')^2} \right]$. Together, $\lambda_{\hat{z}|z}|_{\partial D}$ and $\partial_{\mathbf{n}} \lambda_{\hat{z}|z}|_{\partial D}$ fully describe the shape of the boundary: $\lambda_{\hat{z}|z}$ is the local arc length, and $\kappa = \lambda_{\hat{z}|z}^{-1} + \partial_{\mathbf{n}} \lambda_{\hat{z}|z}$ is the curvature (Appendix C). The orientation of the tangent to the boundary at arc length s is given by $\phi(s) = \int_0^s \kappa(s') ds'$. One can then integrate to obtain the boundary curve $z(\hat{z})|_{\partial D}$. Finally, the value in the interior is determined by Cauchy's integral:

$$z(\hat{z}) = \frac{1}{2\pi i} \oint_{\partial D} \frac{z(\hat{z}')}{\hat{z}' - \hat{z}} d\hat{z}'. \quad (\text{F5})$$

Appendix G: Kinematics of quasiconformal flow

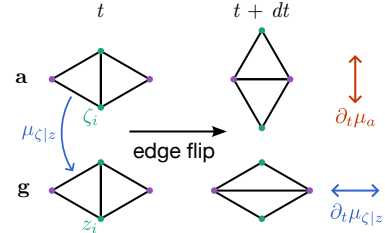


FIG. 8. Illustration of the geometry of Eq. (G4). The adjacency metric represents a triangulation where each edge has length 1, and therefore undergoes a shear deformation if adjacency is changed by an edge flip (T1 transition). The tension metric remains fixed under a T1. As a result, the tension triangle shape acquires anisotropy.

1. Convective derivative of $\mu_{\zeta|z}$

Consider the quasiconformal flow $\zeta' = \zeta + \dot{\zeta} dt$ under dynamics of the adjacency metric; $\partial_{\zeta} \dot{\zeta} = \partial_t \mu_a$. We calculate how $\mu_{\zeta|z}$ changes under this flow while holding the tension metric \mathbf{g} fixed. To find the new Beltrami coefficient $\mu_{\zeta'|z}$, we need to compose the maps $\zeta' \mapsto \zeta$ and

$\zeta \mapsto z$. Drawing the map compositions as a diagram

$$\begin{array}{ccc} & \xrightarrow{\mu_{\zeta|z}} & \\ \zeta & \xrightarrow{\mu_{\zeta|\zeta'} = \partial_t \mu_a dt} & \zeta' \\ & \xleftarrow{\mu_{\zeta'|\zeta}} & \\ & \xrightarrow{\mu_{\zeta'|z}} & z \end{array} \quad (\text{G1})$$

Quasiconformal flow induces $\mu_{\zeta|\zeta'} = \bar{\partial}_\zeta \dot{\zeta} dt / (1 + \partial_\zeta \dot{\zeta} dt) \approx \bar{\partial}_\zeta \dot{\zeta} dt = \partial_t \mu_a dt$. To find the Beltrami coefficient of the inverse of a map, one applies the chain rule:

$$\mu_{\zeta'|\zeta} = -\frac{\bar{\partial}_\zeta \dot{\zeta}'}{\partial_\zeta \dot{\zeta}'} \mu_{\zeta|\zeta'}. \quad (\text{G2})$$

Now composing with the map $\zeta \mapsto z$ gives

$$\begin{aligned} \mu_{\zeta'|z}(\zeta', \bar{\zeta}') &= \frac{\mu_{\zeta'|\zeta} + \mu_{\zeta|z} e^{-i2\phi_{\zeta'|\zeta}}}{1 + \bar{\mu}_{\zeta'|\zeta} \mu_{\zeta|z} e^{-i2\phi_{\zeta'|\zeta}}} \quad (\text{G3}) \\ &\approx \frac{-\bar{\partial}_\zeta \dot{\zeta} dt + \mu_{\zeta|z} (1 + i2\text{Im}[\partial_\zeta \dot{\zeta}]) dt}{1 - \mu_{\zeta|z} \partial_\zeta \bar{v}(\zeta) dt} \\ &\approx \mu_{\zeta|z} - \left(\partial_t \mu_a - i\mu_{\zeta|z} \text{Im}[\partial_\zeta \dot{\zeta}] + \mu_{\zeta|z}^2 \partial_t \bar{\mu}_a \right) dt, \end{aligned}$$

where the phase factor is $e^{-i2\phi_{\zeta'|\zeta}} = (1 - \bar{\partial}_\zeta \dot{\zeta} dt) / (1 - \partial_\zeta \dot{\zeta} dt) = 1 + i2\text{Im}[\partial_\zeta \dot{\zeta}] dt$. The displacement change from ζ to ζ' leads to an additional advective term $\text{Re}[\bar{v} \partial_\zeta] \mu_{\zeta|z} dt$. Taken together, one arrives at

$$\frac{d}{dt} \mu_{\zeta|z} = \frac{\mu_{\zeta'|z}(\zeta', \bar{\zeta}') - \mu_{\zeta|z}(\zeta, \bar{\zeta})}{dt} \quad (\text{G4})$$

$$\begin{aligned} &= \partial_t \mu_g - \partial_t \mu_a + \text{Re}[\dot{\zeta} \partial_\zeta] \mu_{\zeta|z} \\ &\quad + i2\mu_z \text{Im}[\partial_\zeta \dot{\zeta}] - \mu_{\zeta|z}^2 \partial_t \bar{\mu}_a \end{aligned} \quad (\text{G5})$$

The final, nonlinear term can be neglected for weak anisotropy $|\mu_{\zeta|z}| \ll 1$ and captures strain-induced rotation. In conventional Cartesian notation, the total derivative of the tension metric \mathbf{g} can be written as

$$\frac{d\mathbf{g}(\zeta, \bar{\zeta})}{dt} = \mathbf{m} + \left[(\dot{\zeta} \cdot \mathbf{D}) \mathbf{g} - \mathbf{D} \dot{\zeta} \cdot \mathbf{g} - \mathbf{g} \cdot (\mathbf{D} \dot{\zeta})^T \right] \quad (\text{G6})$$

Figure 8 provides a geometric explanation of Eq. (G4). The term $\partial_t \mu_g$ arises from the intrinsic dynamics of z , in addition to the coordinate transformation $\zeta \mapsto \zeta'$.

2. Variation of $|\mu_{\zeta|w}|^2$

In the main text, we argue that T1s relax the “total” Beltrami coefficient $\mu_{\zeta|w}$ of the map from \mathbf{a} -isothermal coordinates ζ to the physical state w . We therefore need to calculate the variation of $\mu_{\zeta|w}$ under a small variation of the adjacency metric $\mathbf{a}(\zeta) \mapsto \mathbf{a}'(\zeta) = \mathbf{a}(\zeta) + \delta \mathbf{a}(\zeta)$. First, note that $\mu_{\zeta|w}$ is independent of \mathbf{g} since the map $\zeta \mapsto w$ bypasses the intermediate (reference) configuration defined by \mathbf{g} [cf. (46)]. Now let ζ' be the \mathbf{a}' -isothermal coordinates, which must satisfy the Beltrami equation $\bar{\partial}_{\zeta'} \zeta' = \mu_{\delta \mathbf{a}}$. Drawing the map compositions as a diagram

$$\begin{array}{ccc} & \xrightarrow{\mu_{\zeta|w}} & \\ \zeta & \xrightarrow{\mu_{\zeta|\zeta'} = \mu_{\delta \mathbf{a}}} & \zeta' \\ & \xleftarrow{\mu_{\zeta'|\zeta}} & \\ & \xrightarrow{\mu_{\zeta'|w}} & w \end{array} \quad (\text{G7})$$

makes clear that the Beltrami coefficient of the new map $\zeta' \mapsto w$ is calculated by composing $\zeta' \mapsto \zeta \mapsto w$ [red path in Eq. (G7)]. We first use that $\zeta \mapsto \zeta'$ is simply the quasiconformal flow induced by $\delta \mathbf{a}$ so $\mu_{\zeta|\zeta'} = \bar{\partial}_\zeta \zeta' / \partial_\zeta \zeta' = \delta \mu_a$. The inverse is obtained using Eq. (G2), giving

$$\mu_{\zeta'|\zeta} = -\frac{\bar{\partial}_\zeta \dot{\zeta}'}{\partial_\zeta \dot{\zeta}'} \mu_{\zeta|\zeta'} = -\frac{\bar{\partial}_\zeta \dot{\zeta}'}{\partial_\zeta \dot{\zeta}'} \delta \mu_a \quad (\text{G8})$$

Since $|\mu_{\zeta'|\zeta}| \ll 1$, the Beltrami coefficient of $\zeta' \mapsto \zeta \mapsto w$ can be calculated by linearizing the Beltrami composition formula Eq. (48):

$$\mu_{\zeta'|w} \approx \mu_{\zeta'|\zeta} + \frac{\bar{\partial}_{\zeta'} \dot{\zeta}}{\partial_{\zeta'} \dot{\zeta}} \mu_{\zeta|w} = \frac{\bar{\partial}_{\zeta'} \dot{\zeta}}{\partial_{\zeta'} \dot{\zeta}} (\mu_{\zeta|w} - \delta \mu_a) \quad (\text{G9})$$

And therefore, we conclude:

$$|\mu_{\zeta'|w}|^2 = |\mu_{\zeta|w}|^2 + (\mu_{\zeta|w} \delta \bar{\mu}_a + \bar{\mu}_{\zeta|w} \delta \mu_a) \quad (\text{G10})$$

$$\Rightarrow \frac{\delta |\mu_{\zeta|w}|^2}{\delta \bar{\mu}_a} = -\mu_{\zeta|w}. \quad (\text{G11})$$